UNINE
UNIVERSITÉ DE
NEUCHÂTEL

Novel Laser Sources for Metrology and Spectroscopy

Thesis presented to the *Faculty of Science* for the degree of
Doctor of Science

Kutan Gürel

M. Sc. in Physics

accepted on 31.08.2017 by the jury:

Prof. Thomas Südmeyer   Director

Prof. Rachel Grange   Examiner

Dr. Stéphane Schilt   Examiner

Neuchâtel, 2017

IMPRIMATUR POUR THESE DE DOCTORAT

**La Faculté des sciences de l'Université de Neuchâtel
autorise l'impression de la présente thèse soutenue par**

Monsieur Kutan GÜREL

Titre:

"Novel Laser Sources for Metrology and Spectroscopy"

sur le rapport des membres du jury composé comme suit:

- Prof. Thomas Südmeyer, directeur de thèse, UniNE
- Dr Stéphane Schilt, UniNE
- Prof. Rachel Grange, ETH Zürich, Suisse

Neuchâtel, le 16 octobre 2017   Le Doyen, Prof. R. Bshary

Keywords - Mots clés

Keywords

quantum cascade laser (QCL), intersubband transitions, mid-infrared (mid-IR), distributed feedback laser, spectroscopy, frequency noise, optical frequency comb, phase noise, low noise, noise reduction, frequency modulation, thermal dynamics, titanium sapphire (Ti:Sapphire) laser, diode pumped solid state laser (DPSSL), ultrafast, femtosecond, carrier envelope offset (CEO), self-referencing, fiber laser, opto-optical modulation (OOM), green laser diode.

Mots clés

laser à cascade quantique (QCL), transitions inter-sous-bandes, infrarouge moyen, laser à rétroaction distribuée, spectroscopie, bruit de fréquence, peigne de fréquence optique, bruit de phase, bas bruit, réduction du bruit, modulation de fréquence, dynamique thermique, laser titane:saphir, laser à corps solide pompé par diode, ultra-rapide, femtoseconde, décalage de fréquence entre porteuse et enveloppe, auto-référencement, laser à fibre, modulation opto-optique (OOM), diode laser verte.

Abstract

Lasers have revolutionized the photonics field as a coherent intense light source, capable of performing many tasks. They are widely used in industrial and medical applications, as well as for scientific research. Two important areas of applications are frequency metrology and spectroscopy. Quantum cascade lasers (QCL) cover a wide spectral region in the mid-infrared where most molecules exhibit strong characteristic absorption lines, the so-called molecular fingerprint. QCLs are highly suited for precise molecular spectroscopy, but in their standard configuration, their tuning range is limited. Better frequency tuning mechanisms are required, which can improve many applications. Frequency combs from mode-locked lasers cover a large optical bandwidth and are proven to be ideal tools for frequency metrology. However, many commonly used comb sources have strong drawbacks, in particular with respect to complexity, cost and size. This thesis presents novel directions to improve both QCLs and frequency combs for spectroscopy and metrology.

In the first part of this work, I focus on simple frequency combs generated by Ti:Sapphire lasers. The standard blue-green pumping solutions for Ti:Sapphire lasers are bulky, expensive, have low efficiency, and require a high degree of maintance. Moreover, they usually lack direct

power modulation, which is an advantage for simple implementation of carrier-envelope offset (CEO) stabilization. In this thesis, I investigated the suitability of newly-emerged green laser diodes as pump sources. This work resulted in record-high optical-to-optical efficiencies for diode-pumped Ti:Sapphire lasers. More than 20% with 650 mW of output power for continuous wave, and 15% with 450 mW of output power for mode-locked operation of the laser have been obtained. Green pump diodes exhibit poor spectral and spatial properties compared to other previously used pump sources for Ti:Sapphire frequency combs. In this work, I showed that this challenge can be overcome and demonstrated the first CEO frequency detection and stabilization of a diode-pumped mode-locked Ti:Sapphire laser. Our work indicates the high potential of direct diode-pumping, and might lead to a new generation of cost-efficient and compact Ti:Sapphire lasers.

In the second part of this work, I investigate a novel comb stabilization method for fiber lasers. Today, fiber lasers constitute the majority of commercial frequency combs, because they are compact, easy-to-use and versatile. However, the traditional method of pump modulation is severely limited in feedback bandwidth due to the long gain lifetime, and low-noise sources require additional modulators. Here I demonstrate the first CEO frequency stabilization of an ultrafast fiber laser using opto-optical modulation of a semiconductor chip. Compared to standard pump modulation, the modulation bandwidth is improved by at least a factor of 60, enabling low-noise operation of the fiber laser frequency comb.

In the final study of this thesis, I evaluate a new generation of QCLs with improved frequency tuning properties. Existing frequency tuning mechanisms involve laser mount temperature and laser injection current tuning. Temperature tuning suffers from lack of speed and injection cur-

rent tuning affects the optical output power due to the cross-talk. Here, I study the frequency tuning and modulation properties of a QCL with an integrated resistive heater placed in close proximity to the active region of the laser. This new heater enables fast actuation of the laser frequency with minimal effects on the laser output power. In a simple spectroscopy experiment, I clearly show that this new technique is a highly promising frequency actuator.

Résumé

Les lasers ont révolutionné le domaine de la photonique en tant que source de lumière intense et cohérente capable de réaliser de nombreuses fonctionnalités. Ils sont largement utilisés dans les applications industrielles et médicales, ainsi que pour la recherche scientifique. Deux domaines d'application importants sont la métrologie optique et la spectroscopie. Les lasers à cascade quantique (QCL pour "quantum cascade laser") couvrent une vaste gamme spectrale dans l'infrarouge moyen où la plupart des molécules présentent de fortes raies d'absorption caractéristiques, agissant telle une empreinte digitale des molécules. Les QCL sont particulièrement adaptés à la spectroscopie moléculaire de précision, cependant leur gamme d'accordabilité en longueur d'onde est limitée. De meilleurs mécanismes permettant de moduler leur fréquence permettraient d'améliorer de nombreuses applications. D'autre part, les peignes de fréquences optiques produits par des lasers à verrouillage de mode couvrent une large bande spectrale et s'avèrent être des outils idéaux pour la métrologie optique et la spectroscopie. Cependant, de nombreuses sources de peignes optiques utilisées de nos jours présentent certains inconvénients, notamment au niveau de leur complexité, coût et taille. Cette thèse présente de nouvelles directions pour améliorer d'une part les QCLs et d'autre part les peignes de

fréquences optiques pour la spectroscopie et la métrologie.

La première partie de ce travail est consacrée à un peigne de fréquences optique généré par un laser titane:saphir. Les solutions habituelles de pompage dans le bleu-vert pour les lasers titane:saphir sont volumineuses, coûteuses, peu efficaces et contraignantes en termes de maintenance. De plus, leur puissance optique ne peut généralement pas être directement modulée, ce qui empêche de mettre en œuvre la méthode la plus simple pour l'auto-référencement d'un peigne, c'est-à-dire la stabilisation du décalage de phase entre la porteuse et l'enveloppe des impulsions (carrier-envelope offset en anglais, CEO). Dans cette thèse, l'utilisation de nouvelles diodes lasers émettant dans le vert comme sources de pompage est démontrée. Ce travail a donné lieu à des rendements optiques records pour les lasers titane:saphir pompés par diode. Un rendement de plus de 20% a ainsi été obtenu en régime continu avec une puissance de sortie de 650 mW, et supérieur à 15% en fonctionnement en verrouillage de mode, avec une puissance optique moyenne de 450 mW. Les diodes de pompe vertes présentent de moins bonnes caractéristiques spectrales et spatiales par rapport aux autres sources de pompage utilisées habituellement dans les peignes de fréquence titane:saphir. Dans ce travail, ce défi a pu être surmonté, menant à la première détection et stabilisation de la fréquence CEO d'un laser titane:saphir pompé par diode. Ce travail démontre le haut potentiel du pompage direct par diodes qui peut mener à une nouvelle génération de lasers titane:saphir économiques et compacts.

Dans la deuxième partie de ce travail, une nouvelle méthode de stabilisation est démontrée pour les peignes de fréquence générés par des lasers à fibre. De nos jours, les lasers à fibre représentent la majorité des peignes de fréquence commerciaux, car ils sont compacts, faciles à utiliser

et polyvalents. Cependant, la méthode traditionnelle de stabilisation de la fréquence CEO par modulation du laser de pompe est fortement limitée dans sa bande passante par la longue durée de vie de l'état excité du gain. Par conséquent, des modulateurs supplémentaires sont nécessaires pour réaliser des peignes à faible bruit. Ici, la première stabilisation de la fréquence CEO d'un laser à fibre est démontrée par modulation opto-optique d'un composant semiconducteur. Par rapport à la modulation standard du courant du laser de pompe, la bande passante de modulation est améliorée d'un facteur supérieur à 60, ce qui permet d'atteindre un régime à bas bruit pour les peignes de fréquence basés sur des lasers à fibre.

Dans l'étude finale de cette thèse, une nouvelle génération de QCLs est évaluée, qui présente des propriétés d'accordabilité en fréquence améliorées. Les mécanismes existants de balayage en longueur d'onde utilisent d'une part la température du laser et d'autre part le courant d'injection. Le réglage par la température est lent, tandis que celui par le courant d'injection influence aussi la puissance optique du laser. Ici les propriétés d'accord de fréquence et de modulation d'un QCL par l'intermédiaire d'un élément résistif intégré à proximité de la zone active du laser sont étudiées. Ce nouvel élément permet un contrôle rapide de la fréquence du laser avec des effets minimaux sur sa puissance de sortie. Dans une expérience de spectroscopie simple, le bénéfice de ce nouvel actuateur est démontré.

Contents

List of Figures

List of Tables

Publications

Parts of this thesis are published in the following journal papers and conference proceedings. Some contents are originally copied and reprinted with permission from the corresponding publishers. The copyright of the original publications are held by the respective copyright holders.

Journal publications

1. **K. Gürel**, V. J. Wittwer, M. Hoffmann, C. J. Saraceno, S. Hakobyan, B. Resan, A. Rohrbacher, K. Weingarten, S. Schilt, T. Südmeyer, *"Green-diode-pumped femtosecond Ti:Sapphire laser with up to 450 mW average power"*, Opt. Express 23, 30043-30048 (2015).

2. **K. Gürel**, S. Schilt, A. Bismuto, Y. Bideaux, C. Tardy, S. Blaser, T. Gresch, T. Südmeyer, *"Frequency tuning and modulation of a quantum cascade laser with an integrated resistive heater"*, Photonics 3, 47 (2016).

3. **K. Gürel**, V. J. Wittwer, S. Hakobyan, S. Schilt, T. Südmeyer, *"Carrier Envelope Offset Frequency detection and stabilization of a diode-pumped mode-locked Ti:Sapphire laser"*, Opt. Lett. 42, 1035-1038 (2017).

4. S. Hakobyan, V. J. Wittwer, P. Brochard, **K. Gürel**, A. S. Mayer, S. Schilt, U. Keller, T. Südmeyer, *"Full stabilization and characterization of an optical*

frequency comb from a diode-pumped solid-state laser with GHz repetition rate", Opt. Express 25, 20437-20453 (2017).

5. **K. Gürel**, V. J. Wittwer, S. Hakobyan, N. Jornod, S. Schilt, T. Südmeyer, "*Carrier envelope offset frequency stabilization of an ultrafast fiber laser using opto-optical modulation of a semiconductor chip*", in preperation for Opt. Lett.

6. N. Jornod, **K. Gürel**, V. J. Wittwer, P. Brochard, S. Hakobyan, S. Schilt, D. Waldburger, U. Keller, T. Südmeyer, "*Carrier-envelope offset frequency stabilization of a gigahertz semiconductor disk laser*", submitted to Optica.

7. S. Hakobyan, V. J. Wittwer, **K. Gürel**, A. S. Mayer, S. Schilt, U. Keller, T. Südmeyer, "*Carrier-envelope offset stabilization of a GHz repetition rate femtosecond laser using opto-optical modulation of a SESAM*", submitted to Opt. Lett.

Conference presentations

1. **K. Gürel**, V. J. Wittwer, S. Hakobyan, N. Jornod, S. Schilt, T. Südmeyer, "*Novel techniques for stabilizing fiber laser frequency combs*", Photonics West, San Francisco, CA, February 2018, oral.

2. N. Jornod, **K. Gürel**, V. J. Wittwer, P. Brochard, S. Hakobyan, S. Schilt, D. Waldburger, U. Keller, T. Südmeyer, "*Carrier-envelope offset frequency stabilization of an ultrafast semiconductor laser*", Photonics West, San Francisco, CA, February 2018, oral.

3. **K. Gürel**, S. Hakobyan, V. J. Wittwer, N. Jornod, S. Schilt, T. Südmeyer, "*CEO frequency stabilization of an ultrafast fiber laser by opto-optical modula-*

tion (OOM) of a semiconductor absorber", UFO, Jackson Hole, WY, October 2017, oral.

4. S. Hakobyan, V. J. Wittwer, **K. Gürel**, P. Brochard, S. Schilt, A. S. Mayer, U. Keller, T. Südmeyer, "*Opto-optical modulation for carrier-envelope-offset stabilization in a GHz diode-pumped solid-state laser*", ASSL, Nagoya, September 2017, oral.

5. N. Jornod, **K. Gürel**, V. J. Wittwer, P. Brochard, S. Hakobyan, S. Schilt, D. Waldburger, U. Keller, T. Südmeyer, "*Carrier-envelope offset frequency stabilization of a mode-locked semiconductor disk laser*", ASSL, Nagoya, September 2017, oral.

6. S. Hakobyan, V. J. Wittwer, P. Brochard, **K. Gürel**, S. Schilt, A. S. Mayer, U. Keller, T. Südmeyer, "*Fully-Stabilized 1-GHz Optical Frequency Comb from a Diode-Pumped Solid-State Laser*", EFTF, Besancon, July 2017, oral.

7. S. Hakobyan, V. J. Wittwer, **K. Gürel**, P. Brochard, S. Schilt, A. S. Mayer, U. Keller, T. Südmeyer, "*Opto-optical Modulator for CEO Control and Stabilization in an Yb:CALGO GHz Diode-Pumped Solid-State Laser*", CLEO EU, Munich, June 2017, oral.

8. N. Jornod, **K. Gürel**, V. J. Wittwer, P. Brochard, S. Hakobyan, S. Schilt, D. Waldburger, U. Keller, T. Südmeyer, "*Towards Self-Referencing of a VEC-SEL Frequency Comb*", CLEO EU, Munich, June 2017, oral.

9. S. Hakobyan, V. J. Wittwer, P. Brochard, **K. Gürel**, S. Schilt, A. S. Mayer, U. Keller, T. Südmeyer, "*Fully-Stabilized Optical Frequency Comb from a Diode-Pumped Solid-State Laser with GHz Repetition Rate*", CLEO, San Jose, May 2017, oral.

10. **K. Gürel**, V. Wittwer, M. Hoffmann, S. Hakobyan, S. Schilt, T. Südmeyer, "*First Detection and Stabilization of the Carrier Envelope Offset Frequency*

of a Diode-Pumped Mode-Locked Ti:Sapphire Laser", ASSL, Boston, October 2016, oral.

11. **K. Gürel**, V. Wittwer, M. Hoffmann, S. Hakobyan, S. Schilt, T. Südmeyer, "*First Detection and Stabilization of the Carrier Envelope Offset of a Diode-Pumped Mode-Locked Ti:Sapphire Laser*", Europhoton, Vienna, August 2016, oral.

12. **K. Gürel**, S. Schilt, A. Bismuto, Y. Bidaux, C. Tardy, S. Blaser, T. Gresch, T. Südmeyer, "*New Frequency Tuning and Modulation Mechanism in a Quantum Cascade Laser for Gas Phase Spectroscopy*", LACSEA, Heidelberg, July 2016, oral.

13. **K. Gürel**, S. Schilt, A. Bismuto, Y. Bidaux, C. Tardy, S. Blaser, T. Gresch, T. Südmeyer, "*Characterization of a New Frequency Tuning and Modulation Mechanism for Spectroscopy in a Quantum Cascade Laser*", CLEO, June 2016, oral.

14. S. Schilt, M. Hoffmann, **K. Gürel**, V. Wittwer, T. Südmeyer, "*Optical frequency combs from diode-pumped solid-state lasers*", 8th Frequency Standard and Metrology Symposium, Potsdam, October 2015, oral.

15. **K. Gürel**, V. Wittwer, M. Hoffmann, S. Schilt, T. Südmeyer, "*Diode pumped Kerr-lens modelocked Ti:Sapphire laser generating 450 mW in 58 fs pulses and 350 mW in 39 fs pulses*", ASSL, Berlin, October 2015, oral.

16. **K. Gürel**, S. Schilt, T. Südmeyer, "*Frequency noise and stabilization of quantum cascade lasers* ", Joint annual meeting of Austrian and Swiss Phys. Societies, Vienna, September 2015, poster.

17. **K. Gürel**, V. Wittwer, M. Hoffmann, S. Schilt, T. Südmeyer, "*Green diode pumped Kerr-lens modelocked Ti:Sapphire laser generating 350 mW in 39 fs pulses*", UFO X, Beijing, August 2015, oral.

18. **K. Gürel**, V. Wittwer, M. Hoffmann, C. Saraceno, S. Hakobyan, B. Resan, A. Rohrbacher, K. Weingarten, S. Schilt, T. Südmeyer, *"Diode pumping of ultrafast Ti:Sapphire lasers: power scaling to 200 mW in 68 fs and first noise analysis"*, CLEO EU, Munich, June 2015, oral.

19. **K. Gürel**, M. Hoffmann, C. Saraceno, V. Wittwer, S. Hakobyan, B. Resan, A. Rohrbacher, K. Weingarten, S. Schilt, T. Südmeyer, *"Ultrafast Diode-Pumped Ti:Sapphire Laser Generating 200-mW Average Power in 68-fs Pulses"*, CLEO, San Jose, CA, May 2015, oral.

20. **K. Gürel**, V. Wittwer, M. Hoffmann, C. Saraceno, S. Hakobyan, B. Resan, A. Rohrbacher, K. Weingarten, S. Schilt, T. Südmeyer, *"Noise Analysis of a Diode-Pumped Femtosecond Ti:Sapphire Laser"*, IFCS-EFTF, Denver, CO, April 2015, poster.

21. S. Schilt, L. Tombez, **K. Gürel**, S. Blaser, R. Terazzi, C. Tardy, M. Rochat, T. Südmeyer, *"Frequency noise in quantum cascade lasers: from investigations to active reduction"*, FLAIR, Florence, May 2014, oral.

Chapter 1

Introduction

Since their first demonstration in 1960 by Theodore Maiman [1], lasers found ground in a range of real world applications, other than *death rays*, as was imagined by the newspapers of the time. Scientist could not foresee right away the vast benefits of this invention. It was seen as a solution which brought along many other problems with it. These problems never ended, in fact they greatly increased in number. New types of lasers were discovered, different laser mechanisms and optical guidance in fibers were invented, which popped out new problems. But scientists happily pursued to solve them and found uses to benefit humanity. Numerous new technologies were invented, like high-bandwidth light-speed communication systems, laser surgery, microscopy, metal cutting, quantum teleportation and cryptography, which are just a few in the long list.

1.1 Lasers

Light has a long history in science, that buffled the mind of physicists at every step. Newton interpreted light as a stream of particles in his corpuscular theory [2]. At the same time, Huygens interpreted light as waves [3]. Newton argued that the symmetric nature of reflection and refraction proved light to be particles, since waves do not strictly travel in straight lines. His vision dominated the understanding of light for more than 100 years.

Young's interference experiment in the beginning of the 19th century proved that light was showing wave-like behaviour [4]. Later on, Maxwell's electromagnetic theory predicted that electromagnetic waves have the same speed as light, measured by previous physicists [5]. This was no coincidence.

However, the black body radiation showed contradictions to Maxwell's electromagnetic theory. In the 20th century, Max Plank suggested his quantum theory [6]: "The energy of light is propotional to its frequency, and light exists in discrete quanta of energy". Einstein suggested the concept of photons, calling light as particles with discrete amounts of energy [7]. Until today, quantum mechanics and optics has formed a well known understanding of light, that can act both as a particle and wave.

Einstein predicted *stimulated emission* of photons in population inversion between the upper and lower energy levels of atoms [8]. The stimulated emission creates duplicates of photons with the same frequency and phase, enabling the first demonstration of a laser.

The term *Light Amplification by Stimulated Emission of Radia-*

tion (Laser), was first coined by G. Gould in his laboratory notebook in 1960 [9]. At around the same time, 44 years after Einstein's publication on stimulated emission, the first laser was demonstrated by T. Maiman at Hughes Research Laboratories [1]. It was a solid state ruby laser, pumped by a Xenon flashtube, and produced pulses at a wavelength of 694.3 nm. This first demonstration triggered tremendous interest to what would be a technological breakthrough. In the following five years, many different types of lasers were discovered: Uranium laser by IBM [10], HeNe [11], Nd:YAG [12] and CO_2 [13] lasers by Bell Laboratories, GaAs semiconductor laser by General Electric Labs [14] and Ar:Ion laser by Hughes Aircraft Company [15].
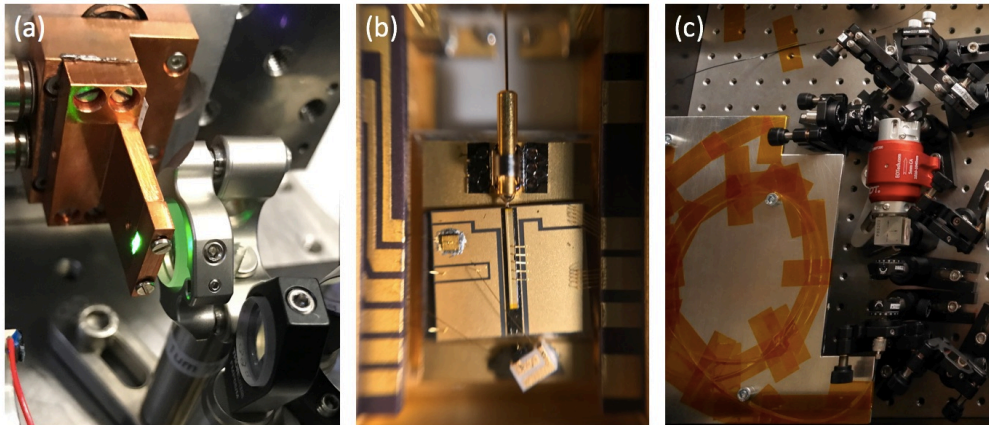
Figure 1.1: Pictures of different types of lasers at Laboratoire Temps-Fréquence: (a) Mode-locked Yb:CALGO solid state laser. (b) Fiber coupled semiconductor laser emitting at 976 nm. (c) Yb-doped mode-locked fiber laser emitting at 1030 nm.

Pictures of some lasers developed or used at Laboratoire Temps-Fréquence (LTF) are shown in Figure 1.1. Different lasers have different pumping schemes. The solid state lasers are optically pumped by another

light source, usually by a laser. Fiber lasers are also optically pumped by other lasers, usually semiconductor lasers. Semiconductor lasers are generally pumped electrically by an injection current.

1.1.1   Continuous wave lasers

The laser can be in its most basic form: continuously pumped to get a continous wave (CW) output. The laser then emits light at a frequency that is matched to a resonator mode, or can consist of multiple different resonator modes. The first CW laser was the HeNe laser discovered in 1961 at Bell Labs [11]. Most CW lasers nowadays are based on semiconductor technology. Very high electrical-to-optical efficiencies as high as 85% can be achieved from semiconductor lasers (also called laser diode) [16]. Mass production on III-V semiconductor wafers and small footprint enable cost-effective laser production. These lasers can be manufactured as distributed feedback lasers (DFB) or distributed Bragg reflector lasers (DBR) that enable single-frequency operation.

The interband transition semiconductor lasers cover wavelengths in the visible-near-IR region, ranging from 380 nm to more than 2 µm.

1.1.1.1   Quantum cascade lasers

For many years, it has been challenging to produce semiconductor lasers emitting in the mid-IR region of the electromagnetic spectrum. The conventional semiconductor lasers rely on electron-hole recombination between the conduction and valence bands, where the emitted photon energy depends on the band gap of the interband transition. The emission wavelength can be set by changing the composition of the semiconductor layers.

Such lasers emitting in the mid-IR region are hard to produce and rely on unmature lead-salt materials.
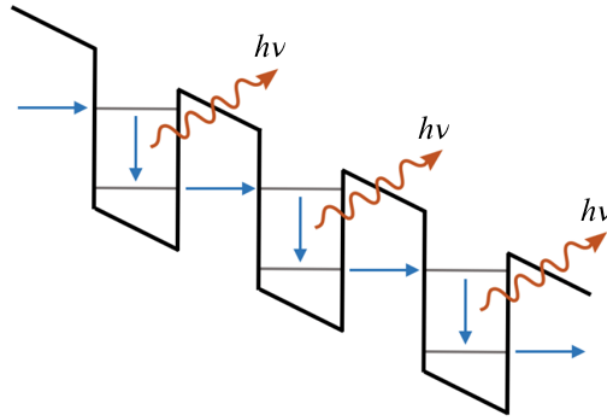
Figure 1.2: Simplified structure of a QCL. Blue lines represent the transmission path of electrons through the cascaded quantum well structure. A photon is emitted at each intersubband transmission.
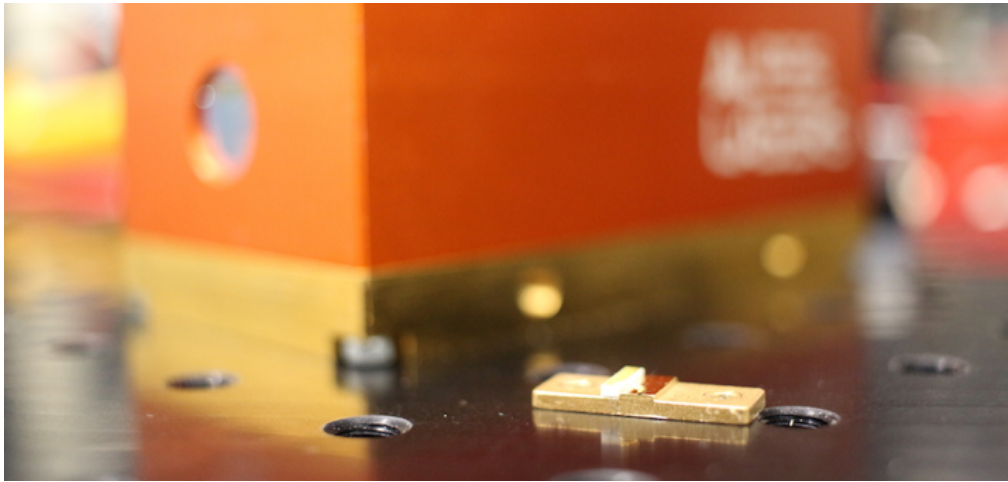
Figure 1.3: Picture of a QCL soldered on its sub-mount. In the background the housing from Alpes Lasers can be seen with a ZnSe window.

In 1994, quantum cascade lasers (QCL) were invented at Bell Laboratories [17]. However, unlike the traditional semicondutor lasers, the

QCLs have a quite different working principle. The electron transition takes place completely in the conduction band, between two energy levels of a quantum well. The quantum well structure is cascaded and an electron is forced to flow through each of these quantum wells, by tunneling in between, as illustrated in Figure 1.2. So from a single electron, some tens of photons can be generated. The most important advantage of QCLs, compared to the traditional semiconductor lasers, is that the photon wavelength does not depend on the bandgap energy, but depends on the quantum well structure that can be engineered accordingly. The laser can be manufactured to produce a wide range of wavelengths from the same material, e.g. using III-V compounds which are widely used for near-IR lasers. A picture of a QCL manufactured by the Neuchâtel company Alpes Lasers can be seen in Figure 1.3.

These intraband transition lasers can emit in the mid-IR and THz ranges, from 2.6 µm to 250 µm.

1.1.2   Mode-locked lasers

Lasers can also operate in pulsed mode, delivering optical pulses with a certain repetition rate, duration and energy. One common way of achieving this is by phase-locking the many modes of a laser resonator (Figure 1.4), hence the term mode-locking [18]. The mode-locking can be achieved passively (passive mode-locking) by use of combination of elements that promote the generation of short pulses inside the cavity, induced by the intra-cavity power fluctuations.

Passive mode-locking of the laser usually results in pulses with a duration shorter than 10 ps. By optimizing the dispersion, nonlinearity,
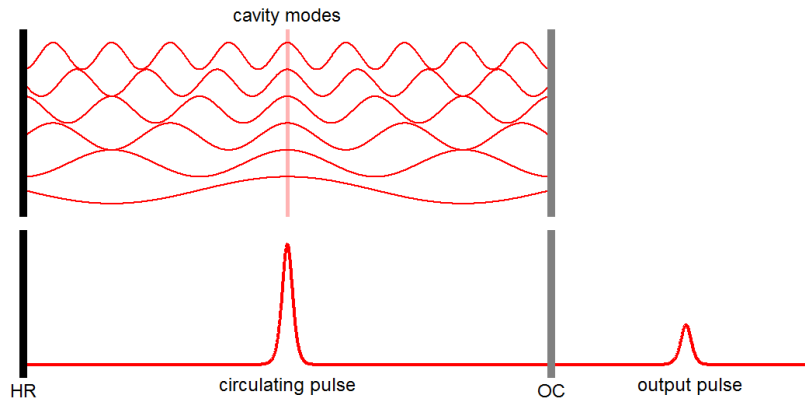
Figure 1.4: Sketch of phase-locked modes in the laser cavity. (HR: highly reflective mirror, OC: output coupler.)

gain and saturable loss, one can create various stability points in the cavity with possibly different laser specifications. The noise initially created by the spontaneous emission in the gain medium gets attracted and evolves towards a stability point at each roundtrip to survive inside the cavity. The laser stays at this stability point, until it is pulled away.

For pulse generation, adding a saturable absorber in the laser cavity is one of the most common methods. The purpose of the saturable absorber is to introduce instantaneous power dependent loss: higher loss at lower power, and lower loss at higher power. This mechanism greatly favors sharp fluctuations of the intracavity power. Each roundtrip increases the effectiveness of the saturable absorber until a pulse survives in the cavity. In the time domain, this results in a train of pulses, seperated by the cavity roundtrip time. In the frequency domain, only the modes allowed by the cavity can exist. After many roundtrips, the modes with appropriate phases survive and their superimposition forms a pulse that propagates back and forth in the cavity. The modes that are out of phase are simply rejected.

There are several options for saturable absorbers in different types of lasers. The most common are nonlinear polarization rotation (NPR) [19] in fiber lasers, semiconductor saturable absorber mirrors (SESAM) [20] and Kerr-lens mode-locking (KLM) [21] in solid state lasers.

During the course of this thesis, I have built and used two types of mode-locked lasers: solid-state Ti-Sapphire and fiber lasers.

1.1.2.1 Ti:Sapphire lasers

Ti:Sapphire laser is by far the most known type of mode-locked laser in the photonics community. Its wide spectral emission capability between 650 nm and 1100 nm [22], and the absence of a patent protection [23] opened the way for its big success. A graph of its tunability range is shown in Figure 1.5. The wide emission bandwidth allowed for the shortest pulses from a mode-locked laser at the time [24]. The Ti:Sapphire laser has been very well developed so far, with demonstrations of sub-two cycle pulses [25], direct octave-spanning output [26], and frequency combs [27].

1.1.2.2 Fiber lasers

The first fiber laser was demonstrated in the beginning of the 1960s by Elias Snitzer in Massachusetts [29]. This eventually paved the way for the development of fiber optic telecommunications. The first passively mode-locked stable-operation fiber laser was demonstrated in 1972 by Ippen, Shank and Dienes [30]. Compared to solid state lasers, fiber lasers have high values of loss, gain, dispersion, and nonlinearity in the oscillator. Fiber lasers have replaced many other types of lasers in the industry, thanks to their simple,
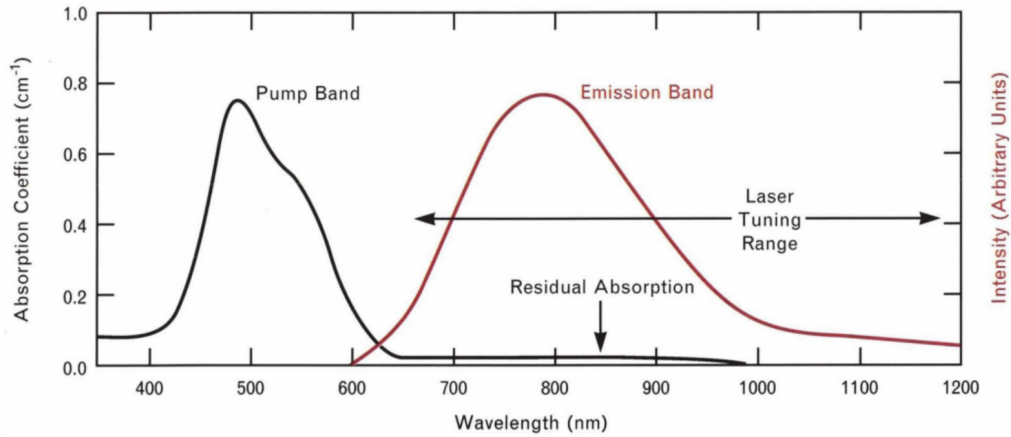
Figure 1.5: Absorption and emission cross section spectra of the Ti:Sapphire crystal. Figure is taken from [28].

reliable and compact nature. Nowadays, there are numerous saturable absorbers enabling mode-locked fiber lasers [19,20,31–33], emitting at various wavelengths ranging from 0.5 µm to 2.9 µm [34].

1.2 Laser applications within the framework of this thesis

The invention of the laser opened up doors to limitless number of applications. Lasers enabled precision, non-invasive operation in all fields of usage. They made a revolution in the medical field. Lasers replaced scalpels in sensitive cutting and tissue removal operations. They are used in dentistry, dermatology, medical imaging, and eye surgery, just to name a few. Lasers hold the primary position in applications such as material cutting, micro-machining, range-finding, and microscopy.

Two of the most important applications of lasers related to this

thesis are frequency metrology and spectroscopy.

1.2.1   Frequency metrology using frequency combs

1.2.1.1   Frequency combs

Frequency combs have gained much attention since the 2005 Nobel prize in physics was awarded to John L. Hall and Theodor W. Hänsch for their contributions to the development of laser-based precision spectroscopy, including the optical frequency comb technique [35, 36]. A frequency comb is an optical spectrum consisting equidistant lines, resembling a hair comb hence the name.

The mode-locked laser is the most popular way of generating these frequency combs. A train of pulses is emitted from a mode-locked laser, each pulse being separated by the cavity round trip time. In the optical frequency domain, the comb teeth are seperated by the laser repetition frequency f_{rep}. There are two degrees of freedom in a frequency comb spectrum: first is the spacing between the comb teeth, f_{rep}. Second is the overall frequency shift of the comb, f_{CEO}, namely the carrier envelope offset (CEO) frequency. The CEO frequency originates from the difference in the phase and group velocities of light in the laser cavity.

If these two frequencies are locked to stable microwave references, then the optical frequency of each comb tooth is accurately known and stable. This stabilization results in a frequency comb, that is a precise ruler in the optical frequency domain. Figure 1.6 depicts the frequency comb in the time and frequency domains.

The stabilization of f_{rep} is generally achieved by a cavity length
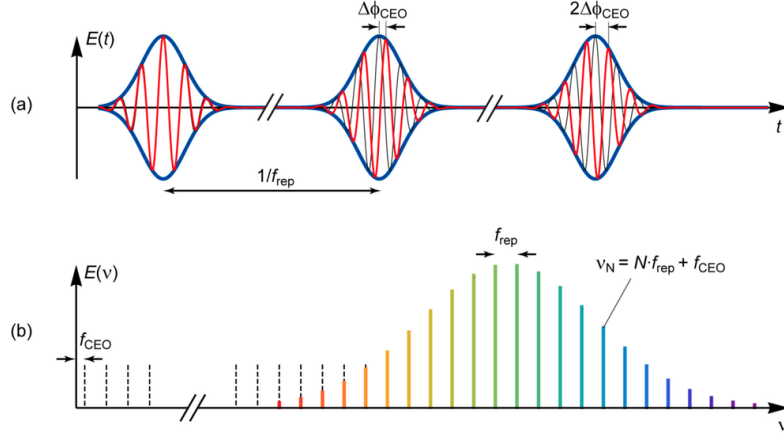
Figure 1.6: (a) Pulse train in the time domain with the CEO phase slippage from pulse to pulse. (b) Optical spectrum of a frequency comb with the CEO frequency at the extrapolated origin of the spectrum. Figure is taken from [37].

actuator, most commonly a piezo-electrical transducer. The stabilization of f_{CEO} is more challenging. The CEO frequency can be measured by a self-referencing technique [38–40]: using an $f - 2f$ interferometer. This interferometer requires a spectrum that covers one octave in frequency, and this is most commonly achieved by external spectral broadening of the pulses in a highly nonlinear medium. The CEO frequency is detected by beating the frequency-doubled lower-frequency end of the comb spectrum with the higher-frequency end, and thus bringing out the offset frequency.

1.2.1.2   Frequency metrology

For a number of applications, the absolute frequency of light needs to be measured. Direct measurement of the wavelength and conversion to frequency is not a preferred method, since it does not result in an absolute measurement. However, the techology is well developed in microwave en-

gineering. Relating the optical frequency to a microwave frequency would enable absolute measurements.

The frequency comb turned out to be the perfect tool! [41] Beating a stabilized frequency comb (with well known optical frequencies, defined by f_{CEO} and f_{rep}) with another the signal to be measured results in an electrical signal in the microwave frequency range. This can be easily measured using a frequency counter. The availability of frequency combs at different spectral regions and the possibility to spectrally broaden them enable a wide selection of optical rulers.

The first frequency comb was demonstrated using a Ti:Sapphire laser, as the technology was well developed around it. There was an important drawback though: the Ti:Sapphire crystal needs to be pumped in the blue-green spectral region, and there was no easy-to-use source for it. So far, all the pump solutions were complex, bulky and expensive. Unlike other wavelengths, there was no laser diode in the blue-green spectral region until recently. For CEO stabilization, it was even more complex: an acousto optic modulator had to be inserted to modulate the pump signal. Although Ti:Sapphire has unique advantages, it became the second choice for frequency combs, when the fiber lasers took over. With the recent emergence of blue and green laser diodes, the Ti:Sapphire laser now has a chance for a come-back. Laser diodes are very small, cheap and easy to modulate. My work with Ti:Sapphire laser focuses on making a compact and stable Ti:Sapphire frequency comb, by implementing green laser diodes as pump source. This proof-of-concept work opens the door to cheaper and simpler Ti:Sapphire frequency combs, as compact and capable measurement tools.

Currently, the fiber lasers constitute the largest portion of the fre-

quency comb market. They emerged fast, as they are quite easy to build and can be made very compact, thanks to the bendable nature of optical fibers. The traditional method for stabilization of the CEO is through pump power modulation, and the modulation bandwidth is mostly limited by the upper state lifetime of the gain material. Although this is not a problem for a Ti:Sapphire laser (with an upper state lifetime of 3.2 µs), for fiber lasers this is a drawback. CEO stabilization through pump modulation results in low bandwidth stabilization, due to the long upper state lifetimes of the common fiber ion dopings, such as *Yb* and *Er*. There are studies involving different types of CEO actuators such as intracavity electro-optic modulators (EOM) [42] and graphene modulators [43]. However EOMs are costly and increase the complexity of the laser and graphene modulators are known to be delicate. In this thesis, I bring in a new method for CEO stabilization of fiber lasers based on opto-optical modulation (OOM) of a semiconductor absorber. This method was initially demonstrated in a solid state laser in our group and yielded excellent performance [44]. Very recently, we also applied a similar approach to another solid-state laser with GHz repetition rate [45]. In this thesis work, I achieved stabilization of the CEO of a Yb-doped fiber laser using OOM of asemiconductor absorber. This will enable affordable and simple solutions for ultra-stable fiber laser frequency combs.

1.2.2   Spectroscopy using QCLs

Spectroscopy studies the light-matter interactions on the basis of optical frequency. The most ordinary example of this is the observation of rainbows. The sun ray interacts with the water droplets in air, the light is

refracted and we witness the intensity of sun light at different colors. In a way, our eyes are primitive spectrometers. We can observe materials with different colors, since the material absorbs some of the light with certain colors. This field has been studied for a long time in the history of science.

Many methods are developed so far to measure and understand the different interactions. The emergence of lasers played a key role in the progress of this field [46]. The laser was a very useful coherent light source with narrow linewidth, wavelength tunability, high output power, and ability to generate ultrashort pulses with broad spectrum when needed.

One common example of an interaction is absorption spectroscopy. Different atoms and molecules absorb electromagnetic waves with certain frequencies. One can send a light beam with a known frequency at the material and simply measure how much of the light is transmitted through. The wavelength of the light can be tuned to measure the response in a wide spectrum and resolve different absorption lines of the material.

The strongest absorption spectrum of most molecules lie in the mid-IR region of the spectrum. For this purpose, narrow linewidth laser sources emitting in the mid-IR spectral region possess great importance as a tool. Measurements in this region provide highly accurate results with distinguishable molecule identification. This is very useful in application where air pollutants or the existence of dangerous gasses need to be monitored.

There are not many available frequency combs in the molecular absorption region. The development of novel laser gain materials and micro resonators is promising, however it is yet to achieve maturity for use in spectroscopy applications [47]. The current fiber and solid state crystal

based frequency combs do not directly emit in this region. These can be frequency converted to longer wavelengths, however this process is cumbersome and adds to the complexity.

On the other hand, QCLs are the perfect tools for spectroscopy of molecules. They can be manufactured to emit in a wide spectral range and can be frequency tuned. They are tiny and can be mass produced. The tunability of QCLs is its most advantageous point for this application. Currently, they are tuned through their injection current or the sub-mount temperature. Both of these methods have disadvantages. Laser current tuning is fast, but also affects the laser output power. Sub-mount temperature tuning has much less effect on the output power, but the laser reacts very slowly to the tuning. Both of these methods are currently used for spectroscopy, but they are not ideal in measurements that rely on speed and optical power.

A resistive heater was implemented in a new QCL design by Alpes Lasers. This heater is in close proximity to the active region of the laser, allowing heat flow in a short time scale. This invention largely eliminates the two mentioned disadvantageous of the traditional frequency tuning methods in QCLs. My work on these new generation QCLs provides introductory insight into future implementations of this method in spectroscopy applications.

1.3 Organization of the thesis

The Neuchâtel area is historically reknown for its passion for understanding time and frequency. The LTF has kept this passion and conducted research

in the areas of time measurement, photonics and metrology. The work carried out in this thesis consists of two strong research areas: optical frequency combs based on diode pumped Ti:Sapphire and fiber lasers for use in metrology and integrated heater tunable mir-IR QCLs for use in spectroscopy.

The content of the thesis is organized as follows:

Chapter 2 presents our work on direct diode laser pumping of Ti:Sapphire lasers. We discuss our characterization of the 1-W multi-mode green laser diodes. The performance of the CW and mode-locked Ti:Sapphire lasers are presented. The noise properties of the laser is discussed.

Chapter 3 presents the realization of the first CEO frequency stabilized, diode pumped Ti:Sapphire laser. The stabilization of the CEO frequency is described and discussed. The noise performance of the Ti:Sapphire laser CEO frequency is analyzed.

Chapter 4 presents the stabilized fiber laser frequency comb using OOM of a semiconductor chip. This is the first time this method is used in a fiber laser and proves to be aan effective solution for generating low noise fiber laser frequency combs. The experiment and the noise performance is discussed.

Chapter 5 describes the new method for controlling and tuning the optical frequency of QCLs. These QCLs are built with an integrated resistive heater close to the active region. We discuss our characterization and test the new tuning mechanism in a preliminary experiment.

Finally, Chapter 6 concludes the thesis with an overview and provides insight into future works.

Chapter 2

Green Diode Pumped Ti:Sapphire Laser

2.1 Introduction

Thirty years after their invention, Ti:Sapphire lasers remain widely used in industry and research [48]. Their broad gain bandwidth ranging between 650 nm and 1100 nm make them the most popular choice for widely tunable laser sources both for CW and pulsed operation [22]. The unique properties of this gain material enabled laser systems for a multitude of applications, such as biomedical imaging, microscopy, optical coherence tomography, spectroscopy, remote sensing and many more [49–53]. The large gain bandwidth is particularly attractive for ultrashort pulse generation. Ti:Sapphire can achieve shorter pulses than any other laser gain material, and Ti:Sapphire amplifiers are currently the most widely used laser technology for strong-field science and attosecond pulse generation [54,55].

The relatively high thermal conductivity of the Ti:Sapphire crys-

17

tal enables high power levels without strong thermal aberrations. However, the saturation power of a Ti:Sapphire laser is relatively high due to its short upper state lifetime [22]. This requires high pump brightness for efficient laser operation. Pumping in the blue-green spectral region is mandatory, which was initially done by Ar:ion lasers and frequency-doubled diode-pumped solid-state lasers (DPSSLs), and in the last years also by frequency-doubled vertical external-cavity surface-emitting lasers (VEC-SELs) [56]. These pump lasers impose a high complexity of the overall system, leading to a lower efficiency than for typical DPSSLs and therefore to higher costs. Furthermore, an important number of applications rely on stabilization of the CEO frequency via fast modulation of the pump power. In the most traditional pumping schemes for Ti:Sapphire lasers, an additional acousto-optical modulator is often required for sufficiently fast control of the pump power [57]. Moreover, the need for versatile and compact frequency comb sources have put Ti:Sapphire lasers in competition with emerging low-cost fiber lasers [58].

Recent developments in indium gallium nitride (InGaN) high-power laser diodes [59] can facilitate the development of simple cost-efficient diode-pumped Ti:Sapphire lasers. Comparisons of previous results with diode-pumped CW and mode-locked Ti:Sapphire lasers are shown in Table 2.1 and 2.2. The first breakthrough was achieved in 2009, when Roth et al. demonstrated the directly diode-pumped CW Ti:Sapphire laser achieving 19 mW [60]. Followed in 2012 by a second breakthrough with the demonstration of the first mode-locking experiment showing 13 mW of average power and 142-fs pulse duration using a SESAM [61]. Initially, a pump wavelength of 452 nm was used, which led to a slow deterioration of the output power due to a pump-induced loss mechanism as the authors

18

have reported [60, 61]. Furthermore, the relatively low pump absorption cross-section in the blue region made efficient laser operation challenging in this first experiment. In a following experiment, the same authors demonstrated 101 mW of average output power with 111-fs pulse duration by adding a second pump, with a total pump power of 2 W [62]. In 2012, Durfee et al. achieved KLM of a Ti:Sapphire DPSSL with 15-fs pulses at 34 mW average power using 2 W of pump at 445 nm [63]. However, in contrast to Roth et al., they did not observe any pump-induced loss in their laser. The highest output power of an ultrafast Ti:Sapphire DPSSL demonstrated so far was 105 mW in 50-fs pulses, which required two 445-nm pump diodes with a total power of 4 W [64]. We also show that the currently available green laser diodes have noise properties that are compatible with frequency comb generation and can be directly modulated in the MHz range.

Author	Pump Power	Pump Wavelength	Average Power	Optical Efficiency
Roth et. al. [62]	2 x 1 W	452 nm	159 mW	8.0%
Tanaka et. al. [65]	2 x 1 W	518 nm	92 mW	4.6%
This work	2 x 1.5 W	520 nm	650 mW	21.6%

Table 2.1: Comparison of continuous wave Ti:Sapphire DPSSL performances

The second breakthrough towards simpler, more cost-efficient Ti:Sapphire sources was recently enabled by the first high power green laser diode providing 1 W of optical power at 525 nm, which was fabricated

19

Author	Pump Power	λ_{Pump}	SA	Average Power	$\Delta\tau$	Opt. Eff.
Durfee et. al. [63]	2 x 1 W	445 nm	KLM	34 mW	15 fs	1.7 %
Roth et. al. [62]	2 x 1 W	452 nm	SESAM	101 mW	111 fs	5.1 %
Young et. al. [64]	2 x 2 W	445 nm	KLM	105 mW	50 fs	2.6 %
				70 mW	15 fs	1.8 %
Sawai et. al. [66]	1 x 1 W	518 nm	SESAM	23.5 mW	62 fs	2.4 %
Tanaka et. al. [65]	2 x 1 W	518 nm	SESAM	44.8 mW	74 fs	2.2 %
This work	2 x 1 W	520 nm	SESAM	200 mW	68 fs	10.0 %
	2 x 1.5 W		KLM	350 mW	39 fs	11.7 %
				450 mW	58 fs	15.0 %
Rohrbacher et. al. [67]	2 x 3 W	450 nm	SESAM	460 mW	82 fs	7.8 %
Backus et. al. [68]	3 x 2 W	447 nm	KLM	350 mW	20 fs	5.6 %
	1 x 4W	465 nm		173 mW	15 fs	4.3 %

Table 2.2: Comparison of mode-locked Ti:Sapphire DPSSL performances (SA: saturable absorber, λ_{Pump}: pump wavelength, $\Delta\tau$: pulse duration)

by Nichia Inc. [69]. The demonstration of the first directly green-pumped Ti:Sapphire DPSSL followed: Sawai et al. achieved 23.5 mW of average power in 62-fs pulses using a 1-W laser diode at 520 nm, and a SESAM for mode-locking [66], corresponding to an optical-to-optical efficiency smaller than 2.5%. The same group later improved this result to 44.8 mW using two 1-W laser diodes [65]. However, in these first proof-of-principle experiments, the power level was too low for many applications, and it remained unclear whether other limiting factors were hindering more efficient ultrafast Ti:Sapphire DPSSLs.

Here, I report on a green-diode-pumped ultrafast Ti:Sapphire

laser, generating up to 450 mW of average power at a repetition rate of 418 MHz with 58-fs pulses. This average power is four times higher than any previously published diode-pumped Ti:Sapphire laser. The simple, compact, and cost-efficient setup makes these lasers highly attractive for applications, for which the previous ultrafast Ti:Sapphire technology has so far been too complex and expensive. The six-fold improvement in optical-to-optical efficiency compared to previous results obtained with green-diode pumping [65,66] indicates that air-cooling and battery-driven operation can also be easily realized. The noise properties of green pump diodes have not been studied and so far, it was not clear if diode-pumping of Ti:Sapphire lasers was a viable alternative to traditional pumping schemes. We show that these green laser diodes qualify in low-noise operation of the pump and Ti:Sapphire laser. Therefore, these results show that green diode-pumped Ti:Sapphire lasers are an outstanding solution for more compact and cost-efficient ultrafast Ti:Sapphire laser systems.

2.2 Experiment

2.2.1 Pump laser diodes

We used two pump laser diodes (model NDG7475 from Nichia Inc, Figure 2.1) each delivering up to 1 W of output power at a wavelength of 520 nm (Figure 2.2), when nominally driven at a current of 1.5 A in a counter-pumping scheme. The diodes were placed in small, simple, compact, and air-cooled copper heat sink housings as seen in Figure 2.3. Optionally the diodes were operated at a current of 2.5 A that is higher than the specified standard operating condition in order to achieve around 1.5 W
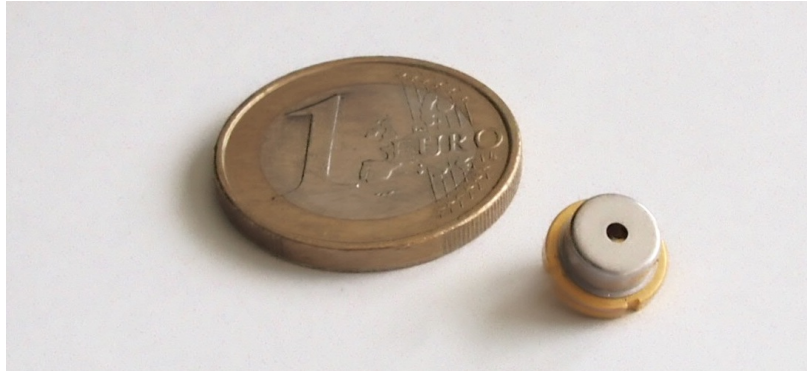
Figure 2.1: Picture of the 1-W green laser diode

output power. However, we did not observe any sign of degradation over more than 100 hours of operation.
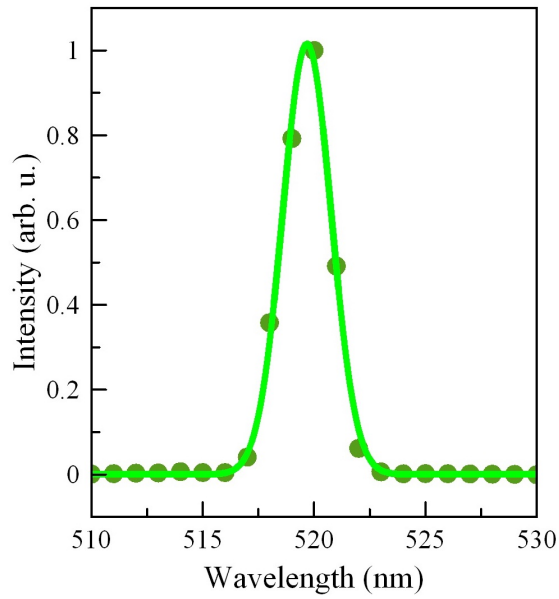
Figure 2.2: Optical spectrum of the 1-W green laser diode (resolution bandwidth=1 nm)

The M^2 of the two pump beams was measured to be 2.7 x 5.5 and 2.2 x 5.4, in the fast and slow axes, respectively, as seen in Figure 2.4. Each pump output was collimated using a lens with a focal length of 4 mm. In
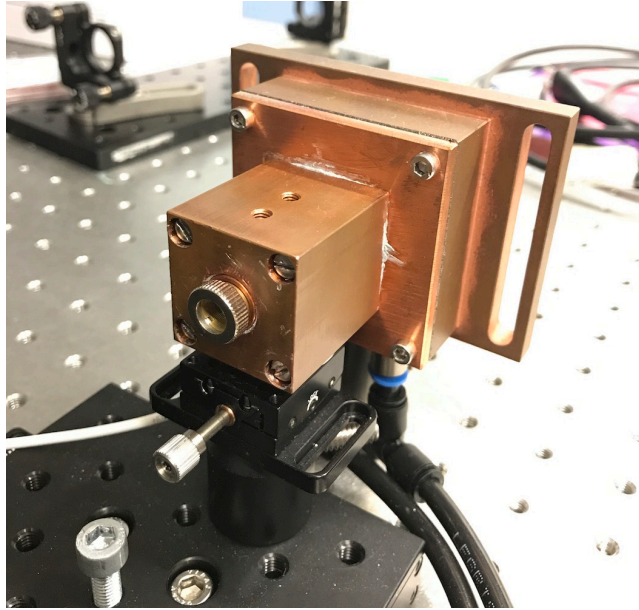
Figure 2.3: Picture of the mounted, water cooled 1-W green laser diode

Figure 2.4: M^2 measurement of the 1-W green laser diode

the first laser configuration, the pump beams were directed through a half-wave plate and a polarizing beam splitter for variable power adjustment

23

onto the crystal. This arrangement was only used in the SESAM mode-locked configuration. Each collimated beam width was enlarged in the slow axis using a set of cylindrical lenses with focal lengths of 15 mm and 100 mm, respectively. The beams were then focused into the gain crystal using 75-mm focal length lenses, followed by the pump mir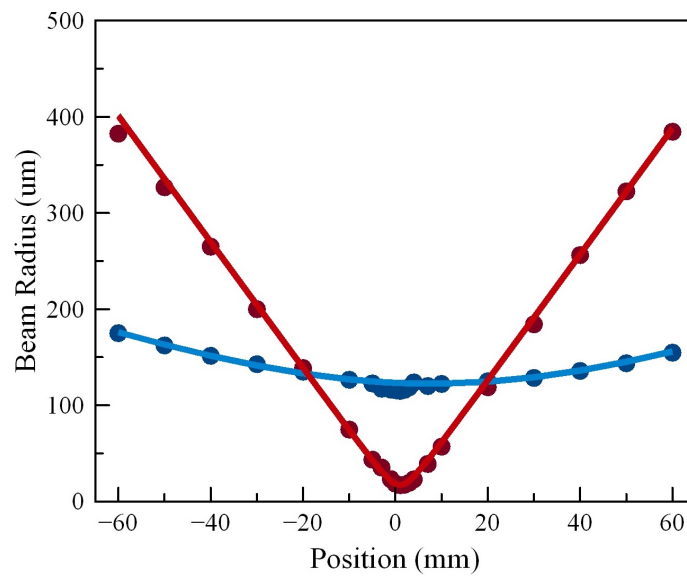rors that have an effective focal length of about -100 mm. The total pump power incident onto the crystal was 2 W in this configuration. In the second configuration, which resulted in the highest CW power level and which was the basis for the KLM results, no variable attenuator was used and the pump diodes were overdriven to achieve a total pump power incident onto the crystal of 3 W. The design of the pump spot size was similar in both configurations. The pump beam profile was measured using a beam profile camera (Dataray Bladecam XHR) and corresponds to a waist radius of 24 µm x 50 µm in the Ti:Sapphire crystal. Pump propagation simulation based on ray transfer matrices is shown in Figure 2.5.

2.2.2   Laser configurations

We used a 4-mm long Brewster-cut Ti:Sapphire crystal (Roditi Ltd.) with 0.25% doping, 4.1 cm^{-1} ($\pm 20\%$) of small signal pump absorption at 532 nm and figure of merit (FOM) of absorption cross-section ratio at 820 nm to 514 nm of 150. The single pass pump absorption was measured to be 86 %. The dichroic pump mirrors have a radius of curvature (ROC) of 50 mm and were placed at 15° with respect to the laser beam and 28 mm away from the beam focus in the crystal. The dispersion due to the crystal was calculated to be +464 fs^2 per cavity round trip. For CW lasing, the cavity was closed at each end with a highly reflective (HR) mirror and an output
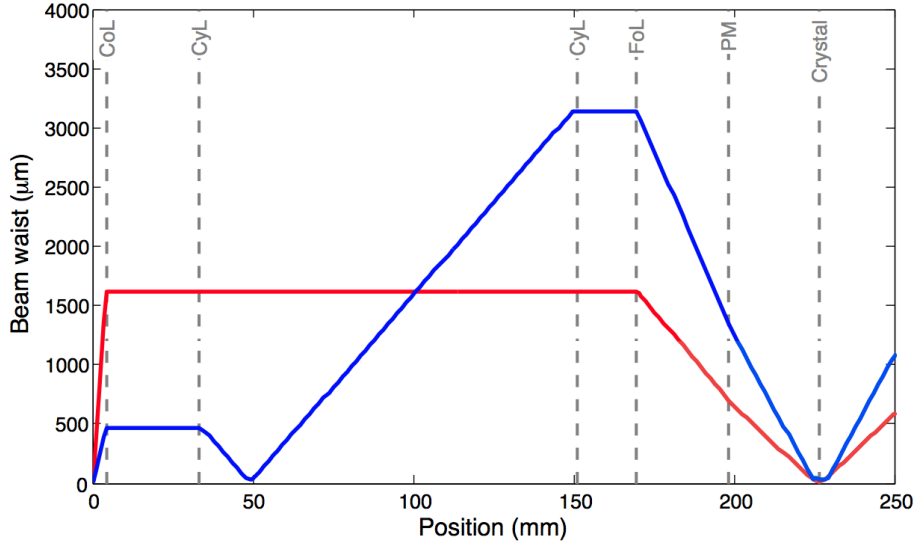
Figure 2.5: Pump propagation simulation in fast (red) and slow (blue) axes. (CoL: collimating lens, CyL: cylindrical lens, FoL: focusing lens, PM: pump mirror.)

coupling (OC) mirror with a transmission of 2%, respectively. The two mirrors were placed at a distance of 160 mm (Figure 2.6(a)). The cavity simulation for the CW configuration can be seen in Figure 2.7.

In order to achieve soliton pulse formation, we introduced two Gires-Tournois interferometer (GTI)-type dispersive mirrors (Layertec GmbH) in one arm (Figure 2.6(b, c)). The GTI-type mirrors are followed by the 2% OC mirror as one end mirror in the cavity, resulting in an arm length of 160 mm. In the other arm, the beam was focused using a mirror (ROC of 150 mm, tilted by 13°) onto either an HR mirror for CW operation, or onto a SESAM (provided by JDSU Ultrafast Lasers AG) that is optimized for 810 nm with a modulation depth of 1%. The total arm length was 185 mm. For the KLM operation, this arm was shortened to around 140 mm and consisted of only a GTI-type mirror as the end mirror (Figure
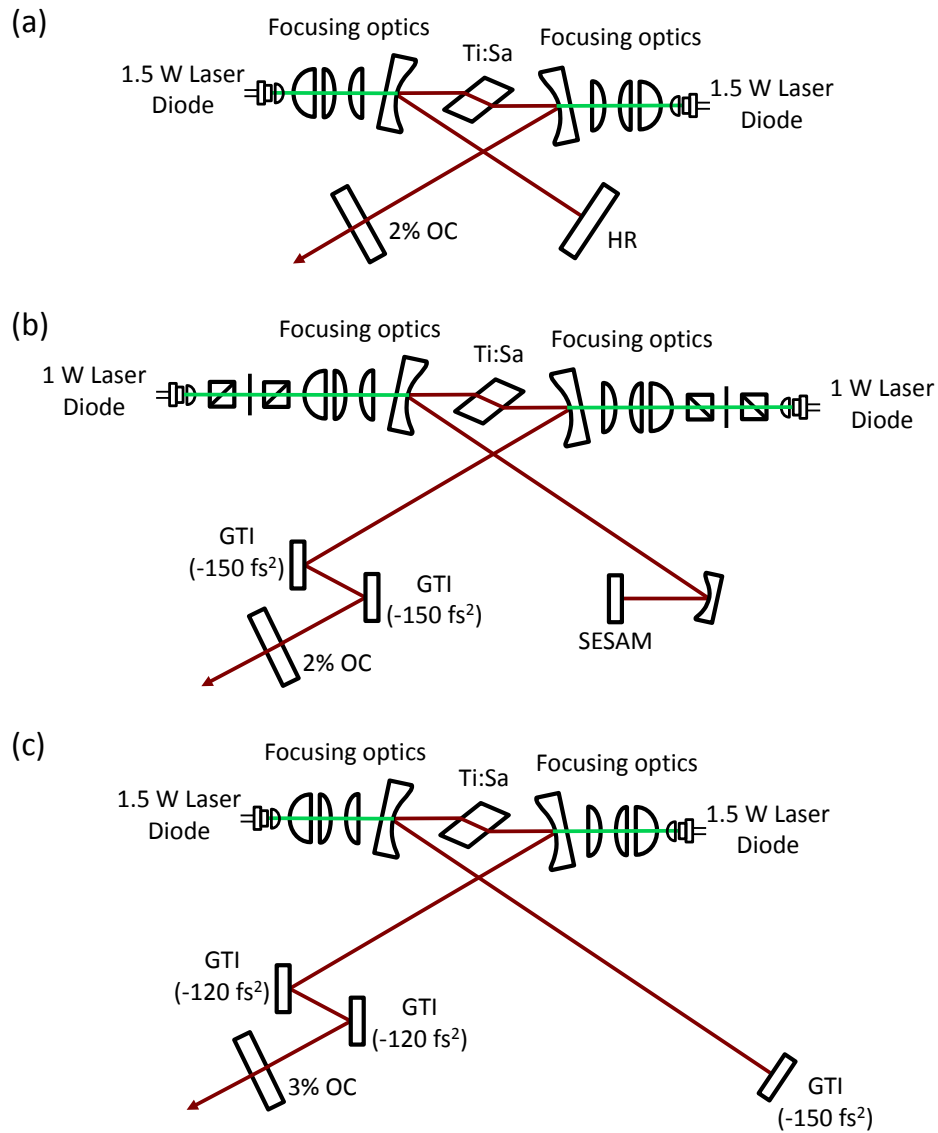
Figure 2.6: Diagram of the Ti:Sapphire laser setup for (a) CW, (b) SESAM and (c) KLM configurations.

2.6(c)), mounted on a translation stage for varying the laser spot size in the crystal and initiating mode-locking. The other cavity arm was lengthened to 165 mm. Cavity simulation for the KLM configuration can be seen

26
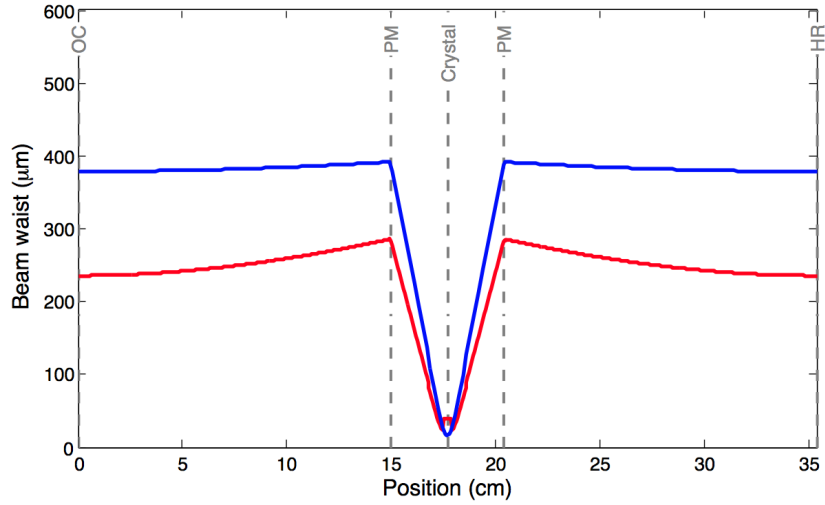
Figure 2.7: CW laser cavity simulation in the sagittal (red) and tangential (blue) axes. (OC: output coupler, HR: highly reflective mirror, PM: pump mirror.)

in Figure 2.8. The inserted negative dispersion for the different cavities corresponds to -600 fs^2 for the SESAM mode-locked version and -780 fs^2 and -840 fs^2 for the two KLM configurations, repectively. For KLM, 2% and 3% OC mirrors were used, respectively. A picture of the setup can be seen in Figure 2.9.

In CW and SESAM mode-locking configurations, the laser mode radii are calculated to be 20 µm x 47 µm and 26 µm x 45 µm in the laser crystal, respectively, and 56 µm x 73 µm on the SESAM.
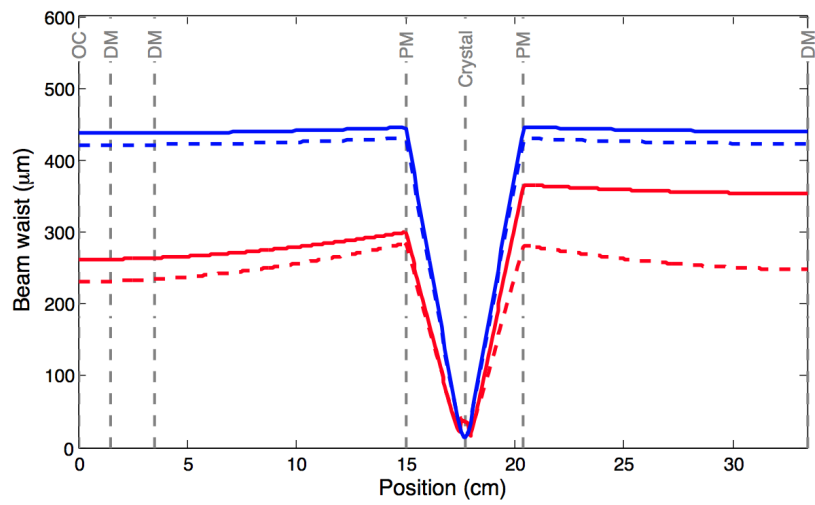
Figure 2.8: Laser cavity simulation in the sagittal (red) and tangential (blue) axes for cases without (dashed) and with (solid) Kerr-lensing enabled. (DM: dispersive mirror, OC: output coupler, PM: pump mirror.)
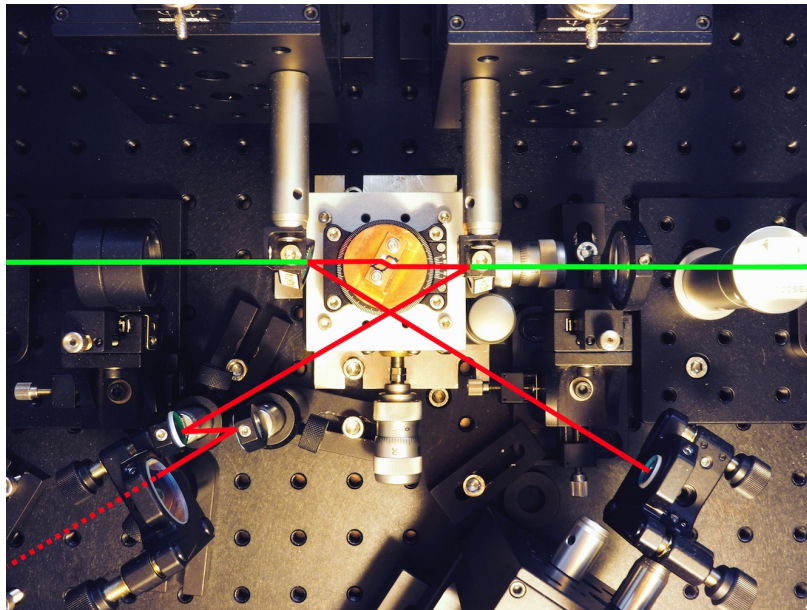
Figure 2.9: Picture of the Kerr-lens-mode-locked Ti:Sapphire laser setup. Green lines indicate the pump beam, and red lines indicate the laser beam.

2.3 Results

2.3.1 CW performance

In CW operation (Figure 2.6(a)), we achieved 650 mW of output power
with 3 W of pump power, resulting in an optical-to-optical efficiency of
22%. The M^2 value of the output beam was measured to be 1.0 x 1.2. We
measured a slope efficiency of 27 % with threshold pump power of 750 mW
(Figure 2.10).
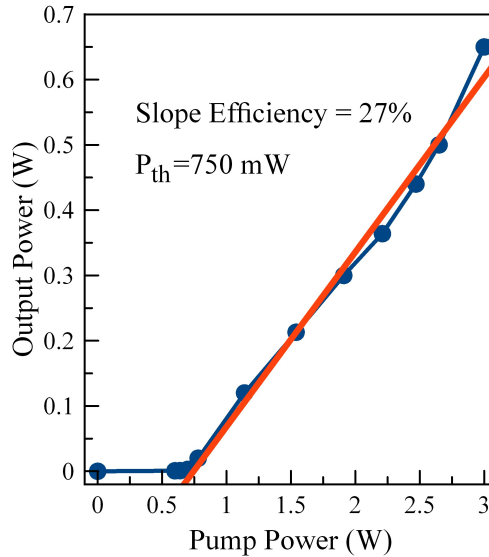
Figure 2.10: Power slope for CW laser configuration of the Ti:Sapphire
laser with a linear fit (red line).

2.3.2 Mode-locked performance

In the cavity configuration for SESAM mode-locking (Figure 2.6(b)), we
achieved stable and self-starting mode-locked operation with an average
output power of 200 mW when pumping at 2 W. The pulses were measured

Figure 2.11: Results for SESAM mode-locked operation with 200 mW output power for 2-W pump power. (a) Auto-correlation trace (solid, black: measurement; dashed, red: fit to auto-correlation of $sech^2$). (b) Optical spectrum (solid, blue: measurement; dashed, red: fit to $sech^2$). (c) RF spectrum around the repetition rate measured with a resolution bandwidth (RBW) of 30 kHz. (d) Enlarged RF spectrum up to 1.2 GHz.

with a background-free intensity autocorrelator (Femtochrome FR-103XL). The full-width at half-maximum (FWHM) of the autocorrelation trace was measured to be 105 fs, resulting in a FWHM pulse duration of 68 fs. The optical bandwidth is 15.6 nm FWHM at a center wavelength of 816 nm (Figure 2.11(a, b)). The radio-frequency (RF) spectrum shows a repetition
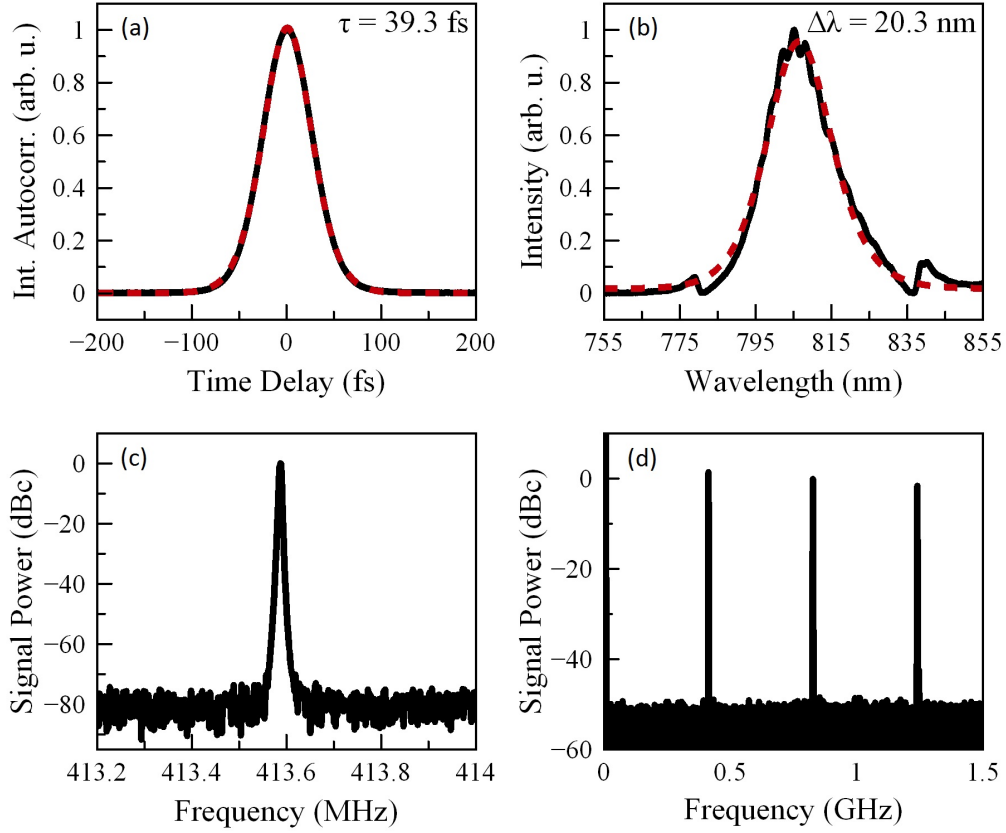
Figure 2.12: Results for KLM operation with 350 mW output power for 3-W pump power. (a) Auto-correlation trace (solid, black: measurement; dashed, red: fit to auto-correlation of sech^2). (b) Optical spectrum (solid, black: measurement; dashed, red: fit to sech^2). (c) RF spectrum around the repetition rate measured with an RBW of 3 kHz. (d) Enlarged RF spectrum up to 1.5 GHz.

rate of 379 MHz, measured using a fast Si detector (Thorlabs DET025AFC) with a bandwidth of 2 GHz and amplified with a 1.8-GHz bandwidth RF amplifier (RF Bay LNA-1835) (Figure 2.11(c, d)). The output beam has a circular beam profile with an M^2 value of 1.2 x 1.2.

In KLM operation (Figure 2.6(c)) with 2% OC mirror, we achieved an average output power of 350 mW and an optical bandwidth of

31

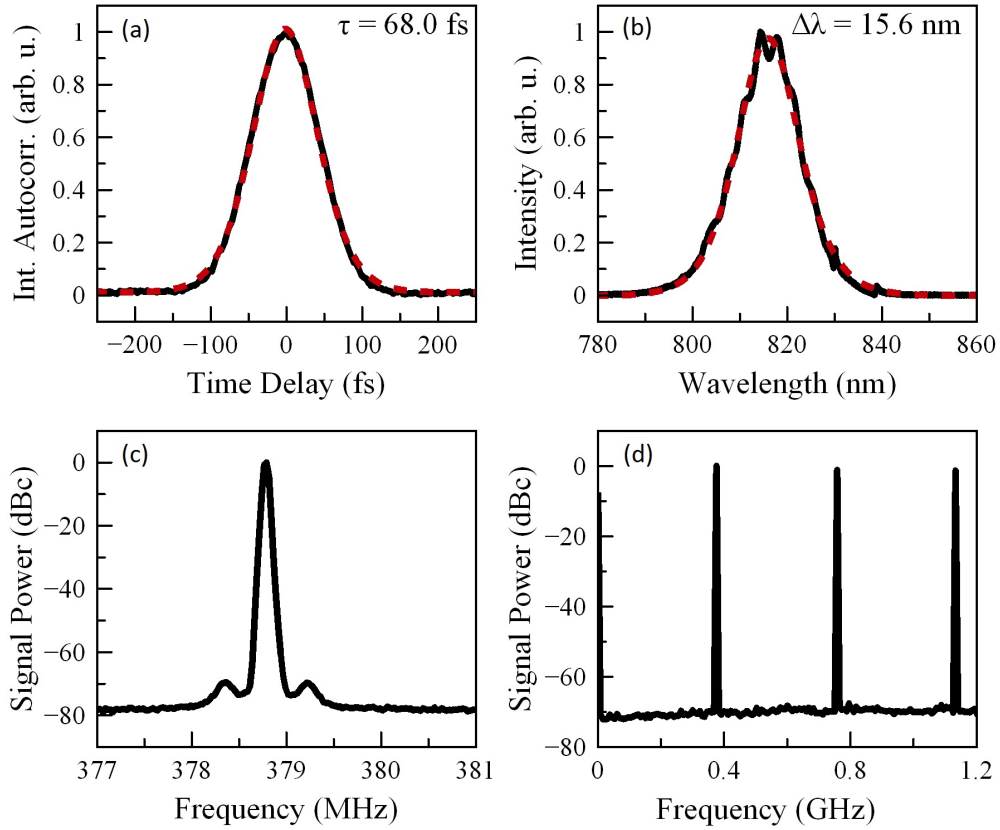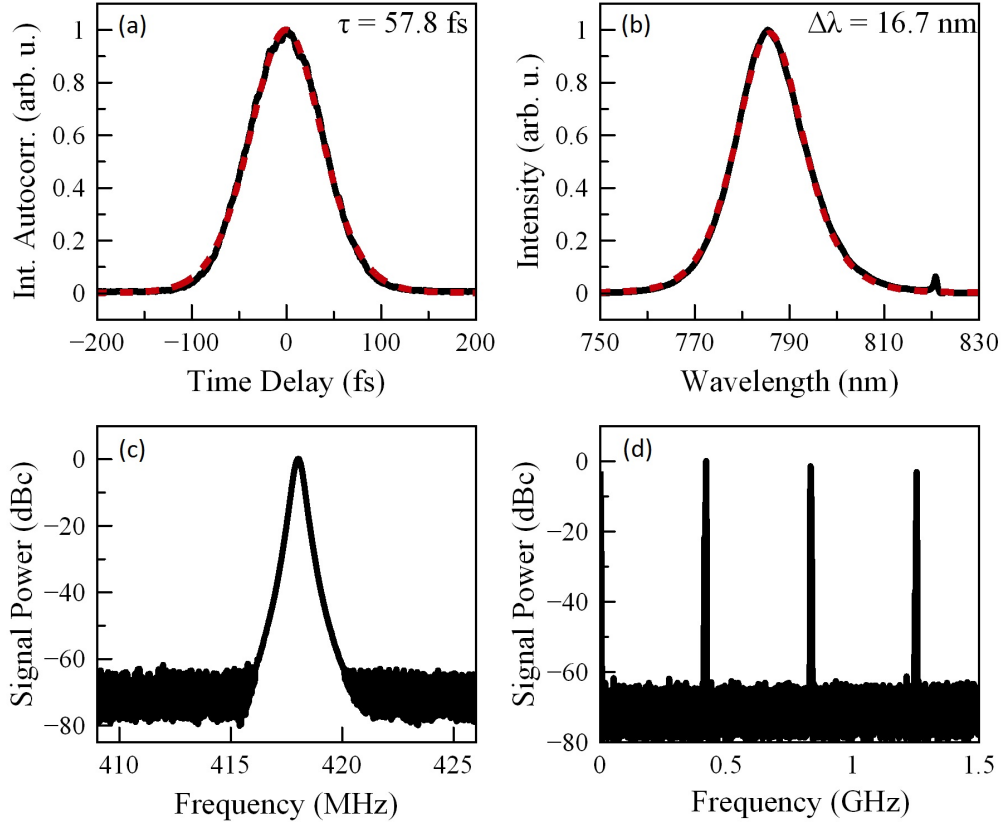Figure 2.13: Results for KLM operation with 450 mW output power for 3-W pump power. (a) Auto-correlation trace (solid, black: measurement; dashed, red: fit to auto-correlation of $sech^2$). (b) Optical spectrum (solid, black: measurement; dashed, red: fit to $sech^2$). (c) RF spectrum around the repetition rate measured with an RBW of 30 kHz. (c) Enlarged RF spectrum up to 1.5 GHz.

20 nm at a repetition rate of 414 MHz (Figure 2.12(b-d)). The RF spectra are measured using a fast Si detector (Thorlabs DET025AFC) with a bandwidth of 2 GHz and amplified with a 1-GHz bandwidth RF amplifier (Mini-Circuits ZFL-1000LN+). We compensated the dispersion of the OC substrate and the collimating lens by 4 extra-cavity reflections on GTI-type mirrors. The measurement of the autocorrelation fits well to a 39-fs

sech^2-pulse (Figure 2.12(a)). Using 3% OC mirror we obtained 450 mW of average power in 58 fs pulses at a repetition rate of 418 MHz (Figure 2.13), corresponding to an optical-to-optical efficiency of 15%.

2.3.3 Noise analysis

We measured the relative intensity noise (RIN) of the green laser diode operated at 1.5-W of output power and of the Ti:Sapphire laser running in KLM configuration (Figure 2.14). A root-mean-square (RMS) RIN of 0.04% was obtained from this spectrum for pump, integrated from 1 Hz to 1 MHz. This noise level is comparable to the value of around 0.02% integrated from 2 Hz to 625 kHz reported for commercially-available standard Ti:Sapphire pump lasers [57]. For the Ti:Sapphire laser, we achieved an RMS RIN of 0.02%, integrated from 1 Hz to 10 MHz. This noise level proves that ultra-low noise operation from diode-pumped Ti:Sapphire lasers is possible.

2.4 Conclusion

We demonstrated the highest power from any diode-pumped Ti:Sapphire solid-state laser, achieving 650 mW power in CW and 450 mW of average power in mode-locked operation with 58-fs pulses. Our results clearly show that Ti:Sapphire DPSSLs can efficiently operate at the current state of In-GaN laser diode technology. The current configuration with two pumps can be further improved by using more pump diodes in a parallel co-pumping configuration to significantly increase the power levels for compact ultra-fast Ti:Sapphire lasers. We showed low noise operation of the pump diodes
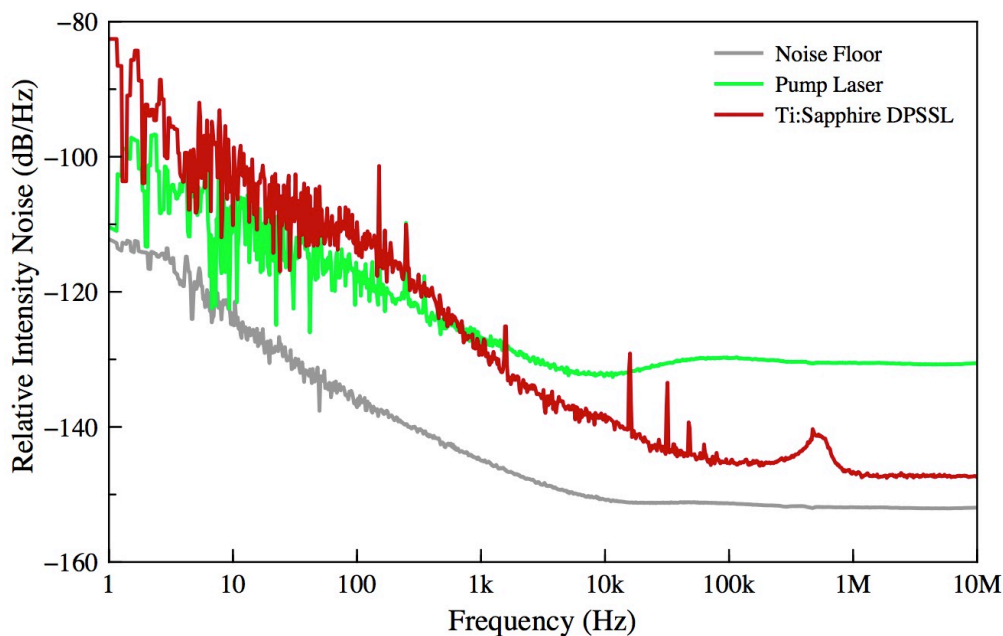
Figure 2.14: Relative intensity noise of the Nichia green laser diode (green) operated at 1.5 W of output power, Ti:Sapphire laser running in KLM operation (red) plotted along with the measurement noise floor (gray).

with an RMS RIN of 0.04%. For the Ti:Sapphire laser, we achieved ultra-low noise operation with an RMS RIN of 0.02%, integrated from 1 Hz to 10 MHz. We expect that low cost, compact, air-cooled Ti:Sapphire lasers will soon be available for applications, both operating in the CW and ultrafast regimes. An interesting advantage for ultrafast oscillators will be the possibility for CEO stabilization in a simple way, either by direct pump current modulation or SESAM opto-optical modulation [44].

Chapter 3

Carrier Envelope Offset Frequency Stabilization of a Diode-pumped Ti:Sapphire Laser

3.1 Introduction

The stabilization of the CEO frequency and the realization of optical frequency combs was a major breakthrough in optical science and photonics. Optical frequency combs can serve as extremely accurate rulers in the frequency domain and provide a phase-stable link between microwave and optical frequencies [27,38,39]. They have been enabling an impressive progress in a wide scientific range, for instance precision metrology [41] and spectroscopy [70], calibration of astronomical spectrometers [71,72], waveform synthesis [38], stable microwave generation [73] and optical clocks [74].

The first stable frequency combs were generated from ultrafast Ti:Sapphire lasers [27]. The emission bandwidth of Ti:Sapphire extends from 650 nm up to 1100 nm, which makes it one of the best suited materials for ultrashort pulse generation [22]. It requires pumping in the blue-green region of the spectrum, which until recently required complex and expensive laser systems. Initially, Ti:Sapphire crystals were pumped by Ar:Ion lasers, which are very unpractical because of their limited lifetime and low wall-plug efficiency, which is typically in the range of 0.1%. Today, they have been mostly replaced by frequency-doubled solid-state lasers, which reach tens of watts of output power with single-mode transverse beam quality. However, their cost, complexity and size is a major disadvantage for Ti:Sapphire lasers compared to ultrafast laser systems that can be directly diode-pumped like Yb- and Er-doped fiber and solid-state lasers [75], which are currently the dominant techniques for frequency combs [37].

The recent development of blue and green laser diodes [69] finally enabled simpler and cheaper pumping options for Ti:Sapphire lasers. In Chapter 2, I have described a green diode-pumped mode-locked Ti:Sapphire laser reaching output powers of 650 mW in continuous wave and 450 mW in mode-locked operation, which is sufficient for many application areas. However, the spectral purity and spatial beam quality of the blue and green laser diodes are significantly worse than frequency-doubled solid-state lasers, which typically operate in the fundamental transverse-mode. In this chapter, I report on the first detection and stabilization of the CEO frequency of a diode-pumped mode-locked Ti:Sapphire laser. The stabilization was realized by direct modulation of the pump diode current, rather than using an external acousto-optic modulator, which is often required in Ti:Sapphire lasers pumped by frequency doubled solid-

state lasers [57].

3.2   Experiment & Results

3.2.1   Ti:Sapphire laser

The laser gain is a 4-mm long Brewster-cut Ti:Sapphire crystal with 0.25% weight doping, 4.1 cm^{-1} ($\pm 20\%$) of small signal pump absorption at 532 nm and a FOM of 150 for the ratio of the absorption cross-section at 820 nm and 514 nm. The cavity follows an X-shape configuration with the gain crystal pumped from each side by a green laser diode (model NDG7475 from Nichia Inc.). The pump diodes are packaged in 8-mm TO cans and can each deliver up to 1.5 W of output power, running at 12% wall-plug efficiency. We mounted them into copper heat sinks, which are water-cooled at 15°C. The two pump beams have M^2 values of 2.7 x 5.5 and 2.2 x 5.4 in the fast and slow axes, respectively. The diodes emit at a central wavelength of 520 nm with a bandwidth of around 2.5 nm. The pump configuration consists of a 4-mm focal length collimating lens, followed by an expanding telescope in the slow axis and a focusing lens with 75-mm focal length. More details on the pump configuration can be found in Chapter 2.

A scheme of the laser cavity is shown in Figure 3.1. Compared to the realization presented in Chapter 2, the resonator is extended in the cavity arm containing the SESAM to obtain a lower repetition rate of around 216 MHz. This arm also includes a Brewster plate (BP) to generate additional self-phase modulation. The beam is then focused onto a SESAM with a modulation depth of around 1% at 810 nm that acts as
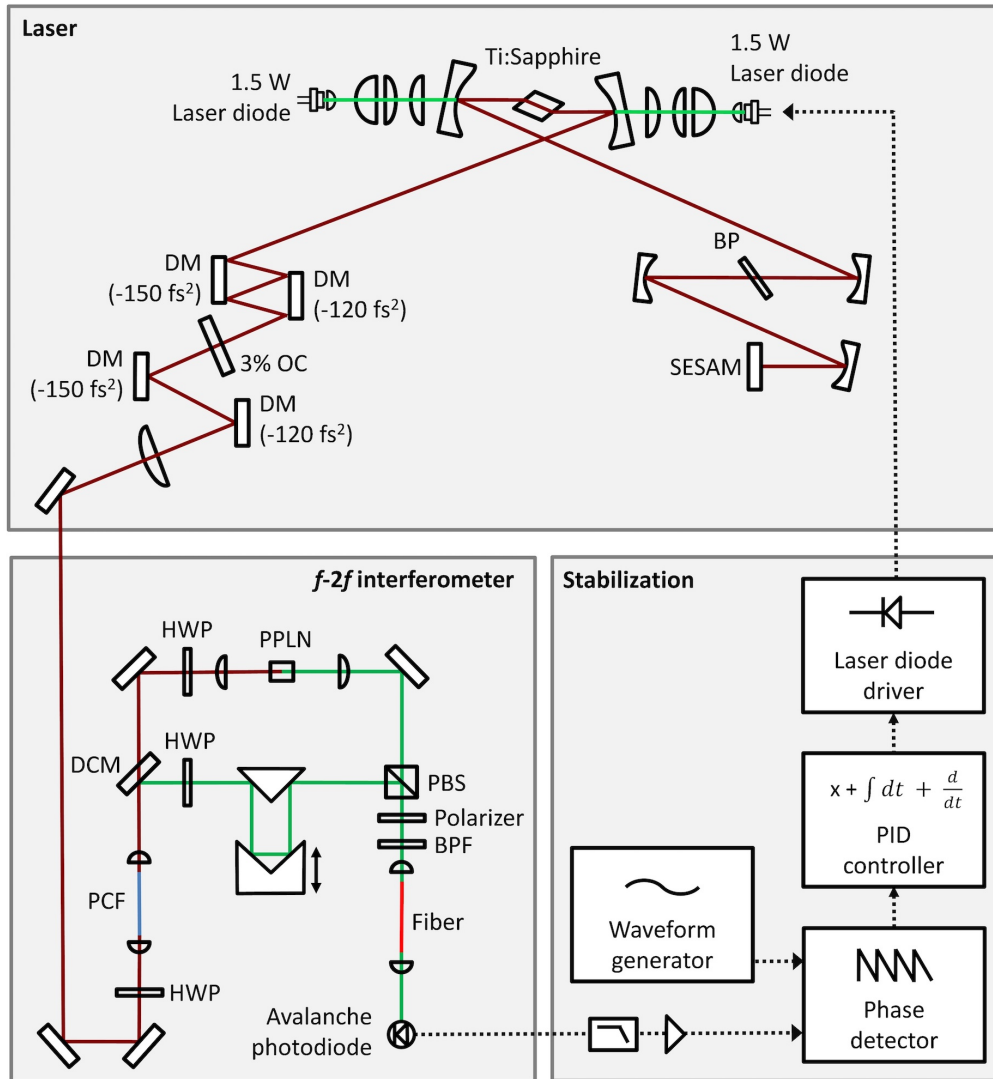
Figure 3.1: Diagram of the complete setup (OC: Output coupler; DM: Dispersive mirror; BP: Brewster plate; HWP: Half wave plate; PCF: Photonic crystal fiber; PPLN: Periodically-poled lithium niobate crystal; PBS: Polarizing beam splitter; BPF: Band pass filter; DCM: Dichroic mirror).

an end mirror. In the other arm of the cavity, the laser beam bounces twice on two GTI-type mirrors with a dispersion value of -150 fs^2 and -120 fs^2,

respectively. This cavity arm ends with an output coupler of 3%. The pulses are then compressed by another set of dispersive mirrors giving a total dispersion of -270 fs^2 to compensate for the material dispersion of the output coupler and of a subsequent lens that collimates the slightly diverging beam. A small fraction of the output power is reflected by a beam sampler for diagnostics.

The laser is SESAM-mode-locked with self-starting operation. SESAM mode-locking was preferred to Kerr-lens mode-locking for its better long-term stability that is required for frequency comb applications. The laser emits 250-mW of average output power with 61-fs pulse duration (Figure 3.2 (a)) at a repetition rate of 216 MHz. The optical spectrum is centered at 815 nm with a full width at half maximum of 12 nm as shown in Figure 3.2 (b).
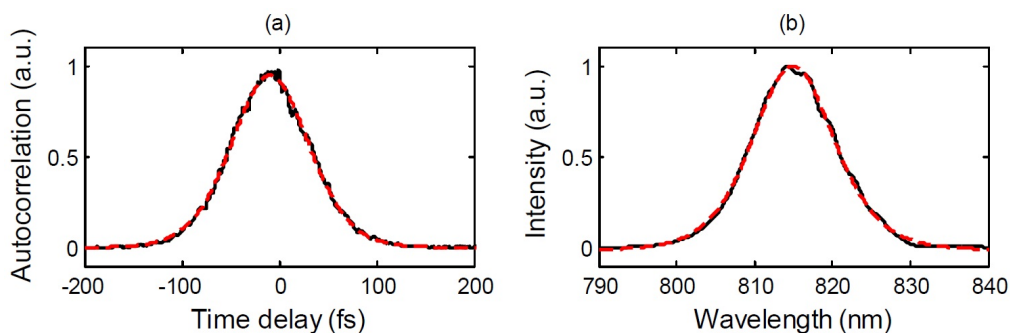
Figure 3.2: (a) Autocorrelation trace of the pulse train (solid, black) with a fit by a sech^2-pulse (dashed, red). (b) Optical spectrum measured at a resolution bandwidth (RBW) of 0.5 nm (solid, black) with a sech^2 fit (dashed, red).

3.2.2 CEO detection and stabilization

The collimated beam was sent through a half wave plate to optimize its polarization and was coupled into a polarization maintaining (PM) photonic crystal fiber (PCF) using an anti-reflection-coated aspheric lens with 4.5-mm focal length. The PCF (model NKT NL-PM-750) is 8 cm long, has 1.8-µm core diameter and a zero-dispersion wavelength of 750 nm. To prevent possible back reflections from perturbing the laser, the fiber ends were angle-cleaved at around 20°. The light exiting the PCF was collimated using another anti-reflection coated aspheric lens with a focal length of 8 mm. An octave-spanning supercontinuum spectrum was generated with significant peaks around 532 nm and 1064 nm as shown in Figure 3.3.
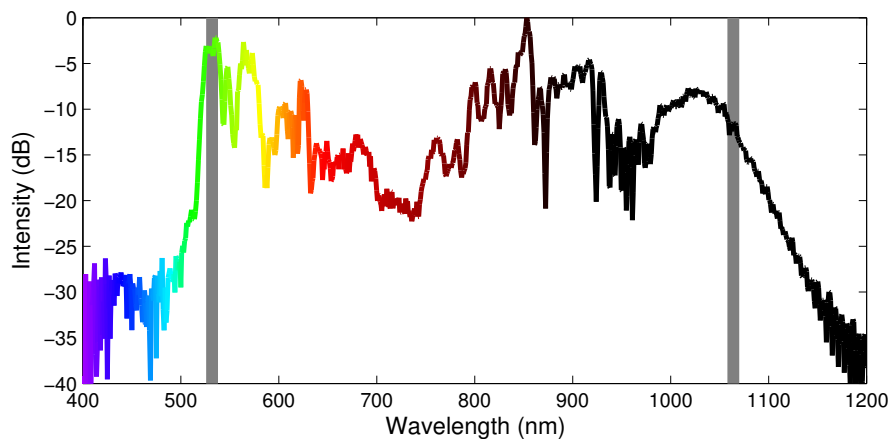
Figure 3.3: Octave-spanning supercontinuum spectrum obtained by launching the laser pulses into an 8-cm long PCF (RBW=1 nm). Gray lines indicate the wavelengths of importance for the interferometer.

The supercontinuum spectrum with 70 mW of average power was launched into a standard $f - 2f$ interferometer, shown in Figure 3.1 lower left panel. A dichroic mirror at the input of the interferometer splits the

40

532-nm component into one arm and the 1064-nm component into the other arm, where it was frequency-doubled in a 10-mm long MgO-doped periodically-poled lithium niobate (PPLN) crystal (from Covesion Inc.) with a poling period of 6.90 µm. The two beams were then recombined in a polarizing beam combiner and passed through a polarizer to align their polarization. A 10-nm-wide spectral band centered at 532 nm was filtered, then the two beams were coupled into a single-mode fiber to enhance their spatial overlap. A beat signal was finally detected in an amplified avalanche photodetector (model APD430A from Thorlabs). The beat signal was measured at around 87 MHz with a signal-to-noise ratio (SNR) of 40 dB at an RBW of 100 kHz (Figure 3.4 (a)). The output signal of the detector was low-pass filtered to extract the lowest frequency CEO beat signal, which was then amplified to a power of around 0 dBm. The amplified CEO beat signal was compared in a digital phase detector (model DXD200 from Menlo Systems) to a reference signal delivered by a waveform generator. The resulting phase error signal was fed into an analog proportional-integral-derivative (PID) controller (model D2-125 from Vescent Photonics) and the amplified correction signal directly controlled the pump laser driver (model 525 from Newport).

The phase noise spectra of the free-running and stabilized CEO beat, measured with a phase noise analyzer (FSWP26 from Rohde-Schwarz), are shown in Figure 3.4 (b). The phase noise is reduced by up to 140 dB at 1 Hz offset frequency when the CEO frequency is locked. The servo bump observed at around 55 kHz corresponds to the stabilization bandwidth, which was limited by the phase shift of the pump diode driver used in this experiment.
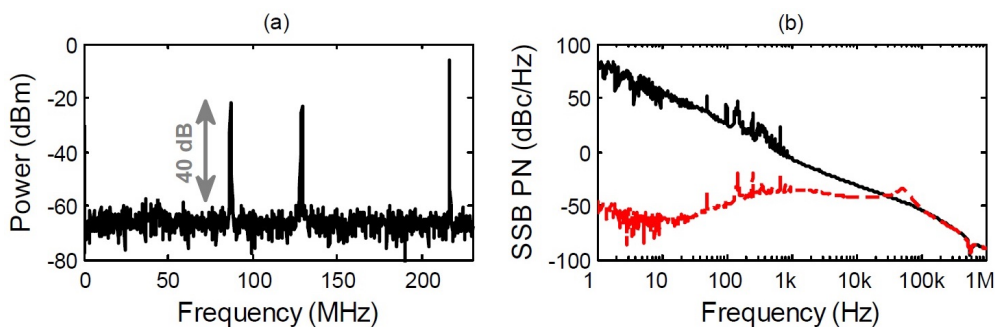
Figure 3.4: (a) RF spectrum of the CEO beat signal with 40-dB SNR obtained at the output of an $f - 2f$ interferometer (RBW=100kHz). (b) Single sideband (SSB) phase noise (PN) power spectral density of the CEO beat when free-running (solid, black) and stabilized (dashed, red)

3.2.3 Modulation capabilities of the green laser diodes

In a separate, later performed experiment, I investigated the modulation capabilities of the 1.5-W green laser diodes. For this purpose, we developed an in-house modulation box capable of delivering an AC current with an amplitude of up to 1 A and a modulation bandwidth of at least 1 MHz. A constant current source was used in parallel with this modulator. We measured the diode-current-to-output-power modulation transfer function in amplitude and phase using a lock-in amplifier (model HF2LI from Zurich Instruments). The measured curves show a -3 dB cutoff frequency of 4 MHz and a phase shift of -90° at 2 MHz as displayed in Figure 3.5. Both the amplitude and phase responses are very flat up to at least 1 MHz. These modulation properties are sufficient to exploit the full modulation bandwidth of the Ti:Sapphire gain for fast CEO control, which is typically in the range of 500 kHz to 1 MHz [76]. The implementation of such a high CEO

modulatiown bandwidth in our laser will enable a significant improvement of the CEO lock.
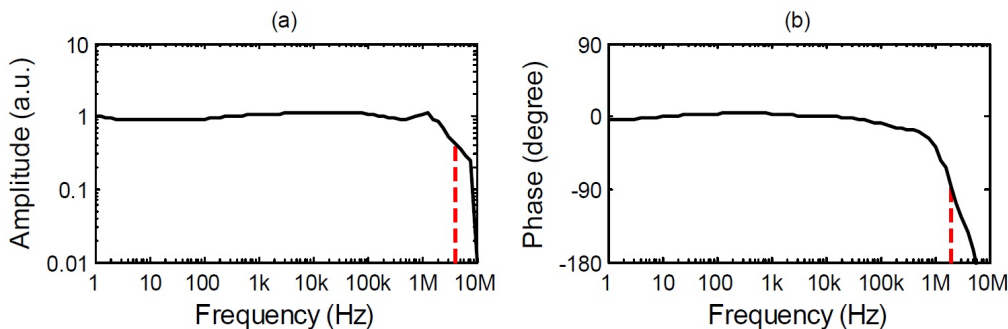
Figure 3.5: Normalized current-to-output-power modulation transfer function of the green pump diode in amplitude (a) and phase (b). The respective bandwidths are 4 MHz (at 3 dB) and 2 MHz (at 90° phase shift).

3.3 Conclusion

In summary, the first proof-of-principle detection and stabilization of the CEO frequency of a diode-pumped Ti:Sapphire laser was demonstrated. I achieved coherent octave-spanning supercontinuum spectrum generation. I measured a CEO beat signal with an SNR of 40 dB in 100-kHz RBW, which is sufficient for phase locking. I stabilized the CEO frequency by direct pump current modulation with a feedback bandwidth of around 55 kHz, reaching a noise reduction of 140 dB at 1 Hz offset frequency. This stabilization scheme circumvents the need for an additional external optical modulator. We investigated the modulation capabilities of these green diodes, demonstrating a bandwidth larger than 1 MHz. This is sufficient for high bandwidth CEO stabilization that is not limited by the pump

power modulation. These results show that expensive and complex green pump sources are not necessary for the realization of Ti:Sapphire frequency combs. Instead, diode laser pumping is a suitable solution for simple, robust, energy efficient and cost-effective Ti:Sapphire frequency combs.

Chapter 4

Carrier Envelope Offset Frequency Stabilization of a Fiber Laser Using Opto-optical Modulation of a Semiconductor Chip

4.1   Introduction

The most challenging aspect for frequency combs concerns the phase-stabilization of the CEO beat. This is traditionally achieved using a phase-locked loop with feedback applied to the pump power of the femtosecond laser, after detection of the CEO beat using non-linear $f - 2f$ interferometry. For example, our Ti:Sapphire comb presented in Chapter 3 was based on this technique. The pump control method is reliable and con-

venient to implement in diode-pumped femtosecond lasers, such as fiber lasers or DPSSLs, for which the injection current of the pump diode can be directly modulated. However, the stabilization bandwidth is typically limited by the upper-state lifetime of the gain material, which is usually in the range of few hundreds of µs to few ms for the most common crystals or glasses gain materials doped with Thulium, Erbium or Ytterbium ions. In order to overcome this limitation, alternative stabilization methods have been proposed, thus improving the locking performance. To this purpose, intra-cavity modulation devices like acousto-optical modulators (AOM), or EOMs can be used. Intra-cavity loss modulation can also be achieved using a reflective graphene electro-optic modulator [43]. In 2013, the LTF demonstrated the first CEO control by opto-optical modulation (OOM) of a SESAM. In this case, an Er:Yb:glass SESAM-modelocked DPSSL operating at a wavelength of 1.5 µm with a repetition rate of 75 MHz was used [44]. An additional CW beam from a diode laser was focused onto the SESAM. This slightly changed its reflectivity as a function of the incident power and acted as a fast loss modulator for the intra-cavity pulses due to the fast SESAM response time. In comparison to the traditional gain modulation via pump control, the OOM showed strong improvements in terms of CEO modulation bandwidth and residual integrated phase noise of the locked CEO beat. Recently, we also implemented a similar approach in another DPSSL operating at the wavelength of 1.05 µm with GHz repetition rate [45]. In this chapter, we investigated the first application of semiconductor-OOM in a fiber laser. To this purpose, we built a femtosecond fiber laser and integrated a VECSEL chip with high modulation depth into the cavity. By pumping the VECSEL chip with a few hundred mW of power, we were able to achieve CEO-stabilization of the Yb-doped fiber

laser.

4.2 Experiment & Results

4.2.1 Fiber laser
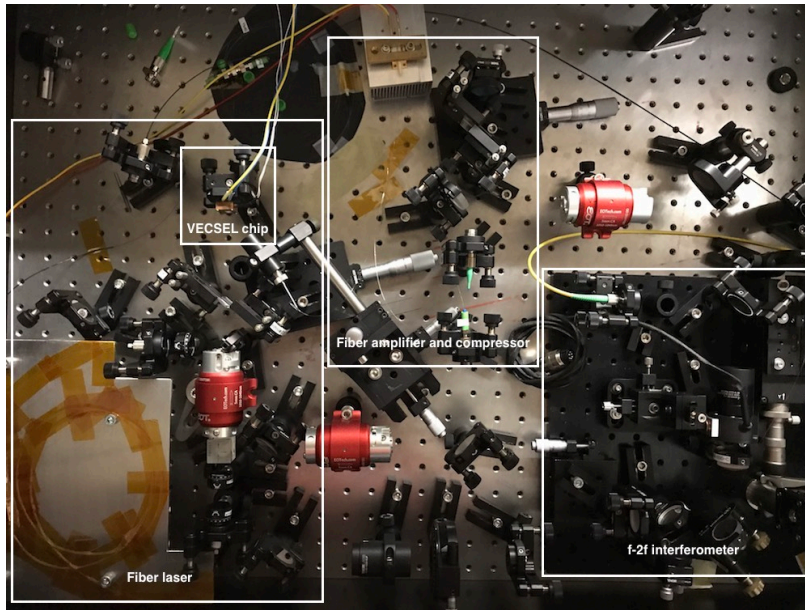
Figure 4.1: Picture of the NPR mode-locked fiber laser, amplifier and the $f - 2f$ interferometer.

The mode-locked fiber laser is based on Yb-doped silica fiber and uses the nonlinear polarization rotation (NPR) method for mode-locking. It contains a 55-cm long Yb-doped gain fiber (Coractive Yb401), a wavelength-division multiplexer (WDM) for pump combining. The fibers are kapton-taped onto an aluminum plate to reduce the influence of thermal fluctuations and air vibrations. A picture of the setup can be seen in Figure 4.1. The free space part consists of two quarter-wave and two half-wave plates for polarization rotation, a polarizing beam splitter for NPR

47
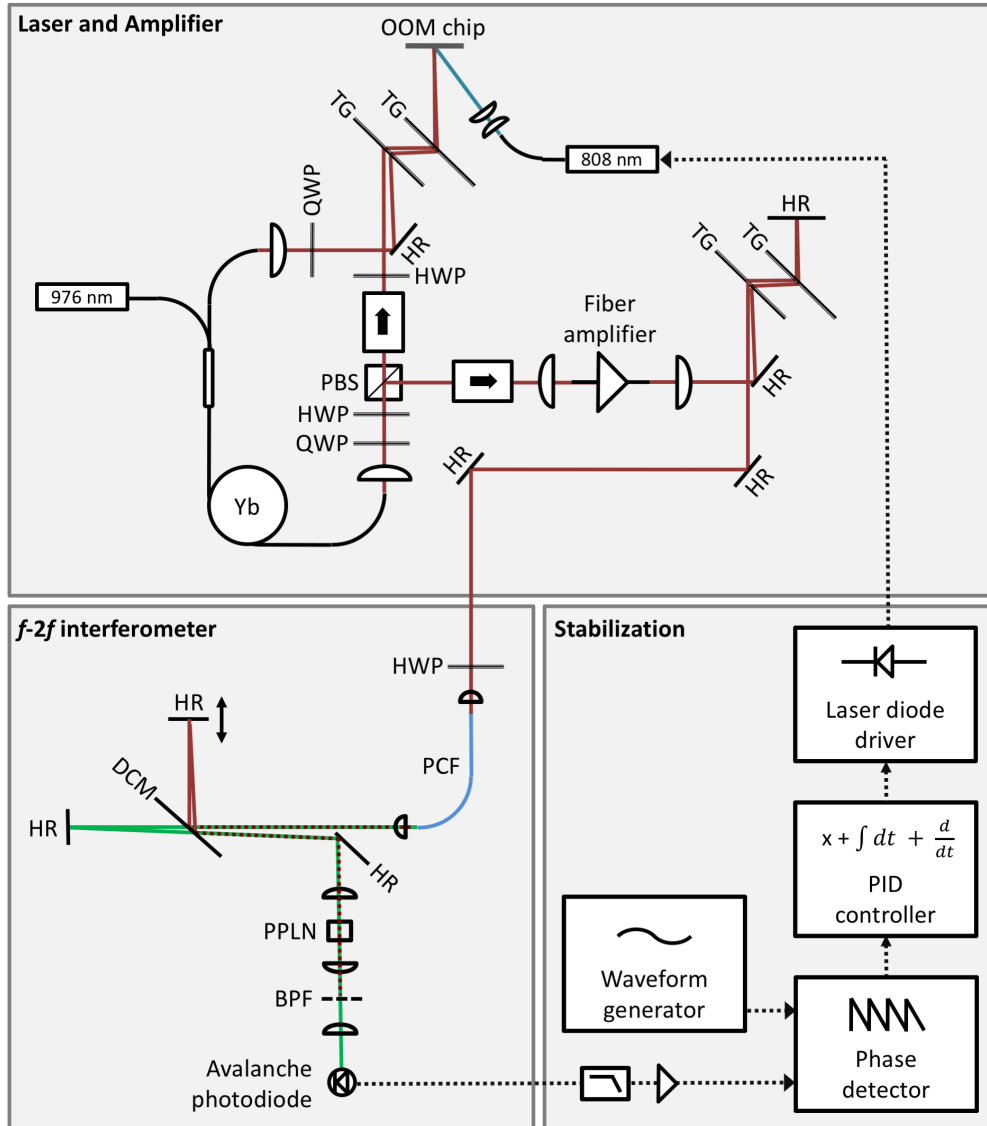
Figure 4.2: Diagram of the complete setup (HWP: Half wave plate, QWP: Quater wave plate, PBS: Polarizing beam splitter, TG: Transmission grating, HR: Highly reflective mirror, PCF: Photonic crystal fiber, DCM: Dichroic mirror, PPLN: Periodically-poled lithium niobate crystal, BPF: Band pass filter).

rejection output, transmission gratings for dispersion management, and an isolator for unidirectional operation. The diagram of the setup is shown in Figure 4.2. The pump is a 976-nm single-mode fiber-coupled laser diode with 500 mW of maximum output power. The total dispersion of the cavity is estimated to be around $+5000\pm2000$ fs^2. The laser operates in the stretched pulse regime at a repetition rate of 125 MHz. The NPR rejection port is used for output coupling. At the output, the laser produces 160-fs pulses with 40 mW of average output power. The pulses are centered at a wavelength of 1030 nm with an optical bandwidth of 26 nm FWHM.

4.2.2   Opto-optical modulation
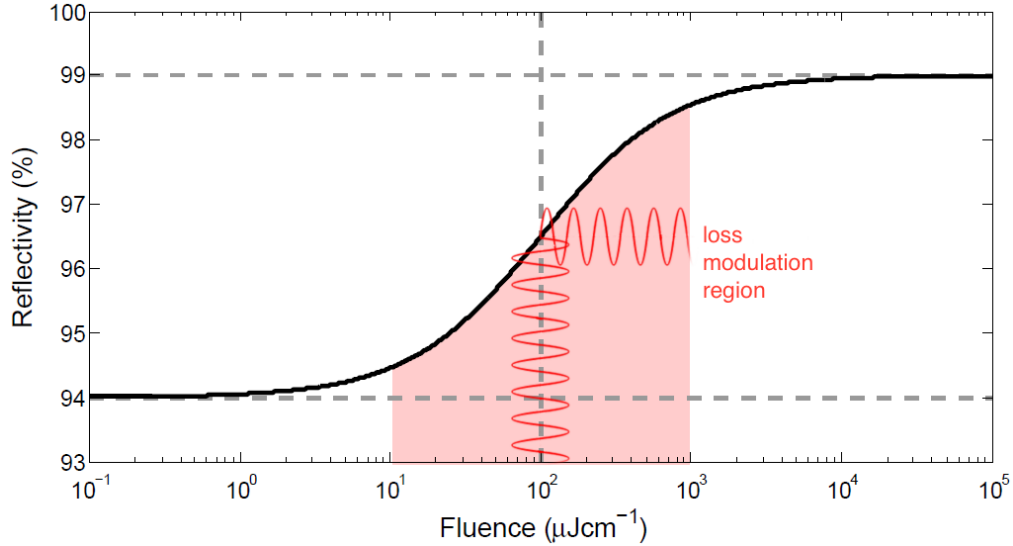
Figure 4.3: Diagram of loss modulation by opto-optical modulation

For the OOM, we inserted a reflective semiconductor absorber into the fiber laser cavity. In order to achieve a high modulation depth, we used a vertical-external-cavity surface-emitting-laser (VECSEL) gain chip as a folding mirror. In this first proof-of principle demonstration, we used a gain

chip that was produced by a commercial manufacturer (M Squared Lasers) and we cannot give detailed information on the design and specifications. The chip is pumped by an 808-nm fiber-coupled laser diode for OOM at an incidence angle of 45°. We only pump it at low intensity of around 300 mW. The laser and pump spot diameters on the chip are around 1 mm. In contrast, in a typical VECSEL, it would be pumped with several watts at this spot size. Therefore, the chip does not reach transparency and it is simply used as a controllable semiconductor absorber with high modulation depth. The low intensity fluence modulation on the semiconductor chip transfers as loss modulation, as shown in Figure 4.3.

4.2.3   Amplification & temporal compression

The NPR rejection output of the laser is passed through an isolator, to perevent possible back reflections from reaching the laser and causing disturbances. Afterwards, the signal is amplified in a polarization maintaining (PM) Yb-doped fiber amplifier. The amplifier has a Yb-doped fiber segment of 80 cm, and can be pumped with up to 1 W of power at 976 nm. The amplified signal is sent into a grating compressor for compression. The grating pair has a separation of around 1 cm and uses dielectric transmission gratings with 1250 grooves/mm (Ibsen Photonics). The compressed output has up to 500 mW average power in sub-100-fs pulses.

4.2.4   CEO detection and stabilization

For the CEO detection, we use the standard $f - 2f$ beat method. The compressed pulses are coupled into a 50-cm long PCF (NKT Photonics
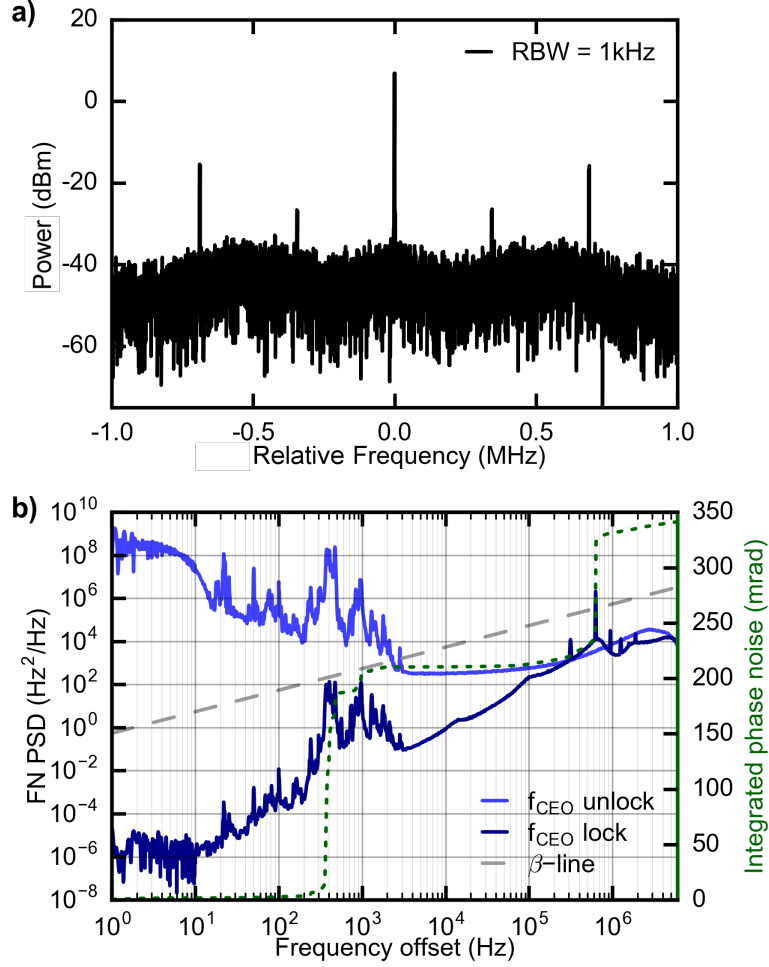
Figure 4.4: (a) RF spectrum of the CEO beat signal with 40-dB SNR obtained at the output of the $f - 2f$ interferometer (RBW=1kHz). (b) Frequency noise (FN) power spectral density of the CEO beat when free-running (light blue) and stabilized (dark blue). The gray dashed line represents the β-separation line [77].

NL-3.2-945) to generate a coherent octave-spanning supercontinuum. Afterwards, we send the beam into the common path $f - 2f$ interferometer. Here the outputs of the PCF is separated by a dichroic mirror into spectral regions below and above 950 nm. Both separated beams are reflected from

distinct mirrors and recombined back at the dichroic mirror. One of the mirrors is mounted on a translation stage that provide an adjustable delay line in order to overlap the two pulses later on. The recombined beam is focused into a MgO:PPLN crystal for second harmonic generation (SHG) from the 1360-nm component of the supercontinuum. The beam out of the crystal is bandpass filtered at 680 nm, which contains the original and the frequency doubled components of the supercontinuum. The filtered beam is then focused onto an avalanche photodiode.

The output of the photodiode is filtered and amplified at 20 MHz to isolate the CEO beat. This signal at 20 MHz is compared to a reference signal in a phase detector. The phase error signal is fed into a PID controller with the output driving the 808-nm laser diode for modulation of the VECSEL chip. We achieve a CEO-stabilization with a bandwidth of 600 kHz, assessed from the servo bump in the CEO frequency noise spectrum (see Figure 4.4 (b)). The CEO frequency is tightly locked as shown in Figure 4.4 (a). The frequency noise displayed in Figure 4.4 (b) results in 342 mrad of residual integrated phase noise, integrated from 1 Hz to 6 MHz.

4.3 Conclusion

In this chapter, we described the first CEO stabilized fiber laser using semiconductor OOM. In this first proof-of-principle experiment, we used a VECSEL chip in order to achieve sufficiently high modulation depth. The OOM is sufficient for full stabilization of the CEO, no further control via the pump power of the fiber laser is needed. Using the standard CEO stablization method based on pump power control of the fiber laser, the

modulation bandwidth is limited to about 10 kHz. In contrast, using OOM, we achieve a feedback bandwidth of 600 kHz, which indicates the high potential of this method for fiber lasers. It enables tight locking of the frequency comb and allows for a residual integrated phase noise lower than 350 mrad. The achieved high feedback bandwidth proves that the simple and cost-efficient semiconductor-OOM is an excellent solution not only for DPSSLs, but also for ultrastable fiber laser frequency combs.

Chapter 5

Frequency Tuning and Modulation of a Quantum Cascade Laser with an Integrated Resistive Heater

5.1 Introduction

QCLs [17] are widely used in high resolution molecular spectroscopy and trace gas sensing applications in the mid-infrared spectral region owing to their unique spectral and wavelength tuning properties. QCLs can be designed to emit in a broad wavelength region ranging from below 4 µm to more than 10 µm based on the mature InP semiconductor material. Singlemode continuous wave operation with output powers reaching more than 100 mW is routinely achieved nowadays at room temperature using a DFB-grating [78], or by placing the QCL chip in an external cavity

configuration [79].

QCLs can be continuously tuned in wavelength through their temperature or injection current. Temperature tuning is rather slow as the QCL temperature is generally controlled with a thermo-electrical cooler (TEC) through a fairly massive sub-mount. However, with a typical temperature-tuning coefficient of $(\Delta\nu/\nu)/\text{T} \approx 10^{-4}/\text{K}^{-1}$ corresponding to around 3 GHz/K in the wavelength range of 8 µm, a large tuning range can be achieved by varying the QCL temperature with a moderate change of the optical output power. Temperature tuning is, thus, mainly used for large but slow frequency sweeping. On the other hand, the QCL wavelength can be rapidly changed with the injection current, at frequencies exceeding 100 kHz [80]. However, the tuning range is limited and current modulation induces a significant change of the emitted optical power. QCL current modulation is widely used in sensitive spectroscopic techniques for trace gas sensing like wavelength/frequency modulation spectroscopy (WMS/FMS) [81, 82] or photoacoustic spectroscopy (PAS) [83]. Each of these techniques involves a modulation of the laser wavelength and a harmonic demodulation of the output signal detected after light-gas interaction (optical signal in WMS or acoustic signal in PAS). A derivative-like signal of the gas absorption feature is thus obtained, which is used to quantify the gas concentration. However, the strong variation in the optical power induced by the QCL current modulation leads to residual amplitude modulation (RAM). This RAM can distort the harmonic signals of a gas absorption line, in particular by inducing an offset in the first harmonic signal ($1f$ detection) that can be detrimental in some applications, for instance when using this signal as an error signal in a feedback loop to stabilize a laser at the center of a molecular or atomic transition. RAM

also results in an asymmetry of the second harmonic signal ($2f$ detection) of a gas absorption line.

A novel tuning actuator in QCLs was recently developed by Alpes Lasers, Neuchâtel, Switzerland. It consists of a small heating element incorporated next to the active region of DFB QCLs [84]. 3D design and scanning electron microscope (SEM) images of this QCL can be seen in Figure 5.1. This integrated heater (IH) is a resistive element driven by an electrical current, which heats the laser via Joules dissipation. This novel design allows the temperature of the active region to be varied much faster than by direct temperature control with a TEC, with a reduced associated change in optical power compared to QCL current modulation. These properties make this new tuning actuator attractive for gas phase spectroscopy applications.
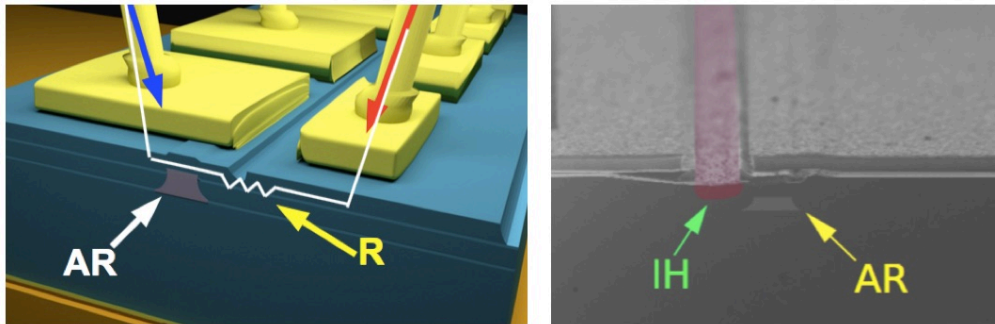
Figure 5.1: 3D design and SEM images of the QCL with IH. The heater extends along the active region. (AR: active region, R: resistor, IH: integrated heater). Images are provided by Alpes Lasers.

The IH current also constitutes a novel channel to apply fast corrections for frequency stabilization and noise reduction in a QCL. Electrical feedback applied to the QCL current is the standard approach to stabilize a QCL to an optical reference, such as a molecular transition or the reso-

nance of an optical cavity, where an error signal proportional to the QCL frequency fluctuations is generated. However, other methods have been demonstrated for frequency noise reduction in QCLs that circumvent the use of an optical reference by exploiting the correlation observed between fluctuations of the optical frequency and of the voltage between the QCL terminals [85]. Using the QCL voltage noise as an error signal to reduce the frequency noise requires another actuator that enables fast internal temperature corrections to be applied to the QCL. The reason is that temperature variations were identified to be the major contribution in the conversion of the terminal voltage noise into frequency noise in QCLs [85]. Such a correction signal cannot be applied directly to the QCL current, as it would simply transpose the QCL voltage noise into current noise without significantly changing the fluctuations of the electrical power dissipated in the laser that are responsible for the frequency noise. Therefore, a fast control of the internal temperature of a QCL for noise reduction was implemented by Tombez et al. by illuminating the top surface of the QCL with a near-infrared laser radiation that could be quickly modulated [86]. A feedback bandwidth in the range of 300 kHz was, thus, obtained. Another approach reported by Sergachev et al., consisted of driving the QCL at constant electrical power instead of constant current, which was realized using fast signal processing of the measured voltage noise [87]. The novel actuator based on an IH is attractive for the realization of such noise reduction loops in a significantly simpler and more compact implementation. However, prior to this, a first step consists in properly characterizing the properties of this new IH actuator.

In this chapter, I present a detailed characterization of the modulation properties of such new IH in a QCL emitting at 7.8 µm. The

reported characterization includes the tuning coefficients, frequency modulation transfer function, as well as the step response. As an example of applications that can benefit from this new actuator, I present a proof-of-principle experiment of WMS of N_2O using a modulation of the IH current, and compare it to the standard approach of injection current modulation.

5.2 Materials and Methods

The QCL manufactured by Alpes Lasers incorporates an integrated resistive heater, as described by Bismuto et al. [84]. The laser is a buried-heterostructure DFB-QCL with a width of the active region of 10.3 µm and a length of 2.25 mm. The integrated heater has a thickness of 2 µm and a width of 8 µm, and is located at a distance of around 1 µm from the active region. The QCL emits in the spectral range between 1273 and 1278 cm^{-1} within a temperature range of 0 °C to 45 °C and delivers up to 80 mW of output power. It was mounted on a copper sub-mount housed in a modified version of the laser laboratory housing (LLH) of Alpes Lasers shown in 1.3, which accommodated the additional electrical connections to drive the IH. The laser and the IH share a common electrical potential at the laser cathode, as shown in Figure 5.2 (a), and were driven by two separate home-made low-noise current sources [85]. These drivers can deliver a current up to 1 A and have a noise spectral density lower than 1 nA/$\sqrt{\text{Hz}}$ at Fourier frequencies higher than 1 kHz. This feature generally enables accessing the frequency noise inherent to a QCL itself, without technical limitation resulting from the QCL current source [88]. The IH has a nearly ohmic response, as shown in Figure 5.2 (b), with an assessed resistance of around 9 Ω that is almost independent of temperature. The

QCL temperature was regulated at the mK level with a double-stage TEC and a negative thermal coefficient (NTC) resistor as temperature sensor, controlled by a home-made temperature regulator.
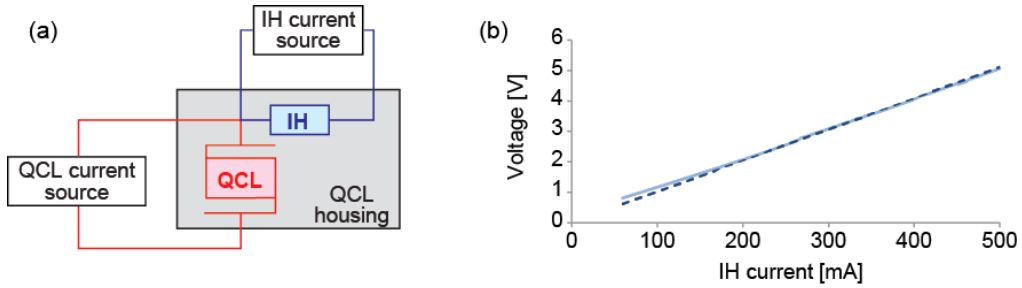
Figure 5.2: (a) Electrical connection scheme of the QCL with IH with their respective current source; (b) current-voltage response of the IH at a sub-mount temperature of 25 °C. The data points (light blue) are well approximated by the pure ohmic response described by the dashed dark blue line.

The frequency tuning, impulse response and modulation transfer function of the laser were measured using a spectroscopic set-up that involved a 10-cm long low-pressure gas cell filled with a nominal pressure of 10 mbar of pure N_2O. However, the imperfect tightness of the cell induced a contamination by air at a total pressure of around 70 mbar (see Subsection 5.3.1), which broadened the absorption lines. The tuning coefficients as a function of temperature, injection current and IH current were obtained by performing a large frequency scan with each actuator and comparing the position of several N_2O absorption lines to their reference frequency extracted from the HITRAN database [89]. The frequency modulation (FM) response of the QCL was measured by tuning the laser to the side of an absorption line used as a frequency discriminator that linearly converted the frequency modulation of the laser (induced by a small modulation of the

injection current or of the IH current) into intensity modulation that was detected with a photodiode (PVI-4TE-5 from Vigo, with a bandwidth of 100 MHz). The resulting intensity modulation was measured in amplitude and phase using a lock-in amplifier and converted into frequency modulation using the measured slope of the absorption line (see Figure 5.3).
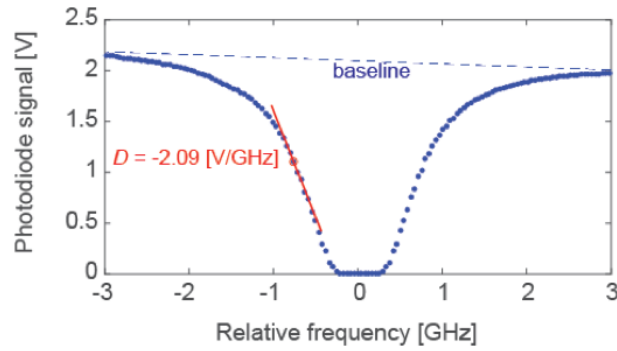
Figure 5.3: Example of N_2O absorption line used as a frequency discriminator to measure the FM response of the QCL. The P11e line of the vibrational band ν_1 of N_2O located at 1275.5 cm^{-1} was used in this case and is shown here. The absorption spectrum was measured by tuning the QCL or IH current and recording the voltage of the photodiode at the output of the reference gas cell. The current axis was converted into a relative frequency using the separately measured tuning coefficient. The operating point is shown by the red circle and the linear range by the red line with a slope D.

Finally, the applicability of the IH for spectroscopy applications was evaluated by the measurement of the first harmonic WMS signal of a N_2O transition obtained by modulating either the IH current or the QCL current at the same frequency of 25 kHz and at different IH or QCL currents.

5.3 Results

5.3.1 Tuning Coefficients

The static tuning coefficients of the QCL were determined from the position of various N_2O absorption lines measured during a scan (see Figure 5.4 (a)) and plotted as a function of the reference frequency extracted from the HITRAN database [89] for temperature (T), injection current (I_{QCL}) and IH current (I_{IH}) tuning, respectively.

Tuning of the QCL injection current or sub-mount temperature results in a nearly linear frequency sweep. On the other hand, the frequency tunes quadratically with the IH current as shown in Figure 5.4 (b), resulting from the Ohm's law dependence. The quadratic response also shows that the IH affects the QCL frequency purely thermally through Joule's dissipation. This leads to a linear response of the laser frequency as a function of the electrical power dissipated in the IH that is displayed in Figure 5.5 in comparison with the temperature and QCL-current tuning curves. The assessed tuning coefficients are 2.9 GHz/K (vs temperature), 37 GHz/W (vs dissipated power in the active region from the QCL current) and 29 GHz/W (vs. dissipated power in the IH), respectively. The power tuning coefficient for the IH is slightly lower than for the QCL current, as the heat dissipation occurs at a slightly larger distance from the active area, thus resulting in a lower heating of this latter region. The corresponding thermal resistance R_{th} associated with the heating of the laser active region by the dissipated power P was determined from the ratio of the power and temperature tuning coefficients, $R_{th} = (\Delta\nu/\Delta P)/(\Delta\nu/\Delta T)$. It amounts to $R_{th,QCL} = 12.8$ (K/W) and $R_{th,IH} = 10$ (K/W), respectively, for the

heat sources resulting from the QCL current and IH current.
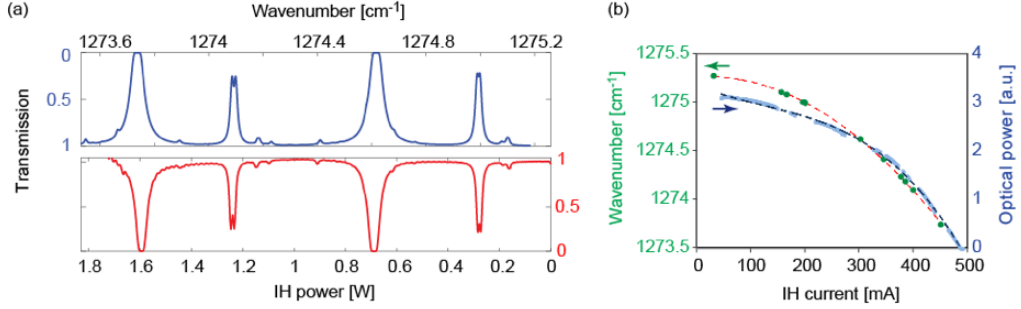
Figure 5.4: (a) N_2O absorption spectrum measured by tuning the QCL with the electrical power dissipated in the IH (bottom spectrum obtained at $T = 25$ °C and $I_{QCL} = 450$ mA) and corresponding N_2O absorption spectrum calculated from HITRAN database [89] for a N_2O pressure of 10 mbar diluted in air (total pressure of 70 mbar) over a path length of 10 cm (upper spectrum). The reference spectrum is inverted for the clarity of the figure. The total pressure in the reference cell that resulted from air contamination arising from the imperfect cell tightness was estimated to be around 70 mbar from comparisons between measured and calculated spectra; (b) corresponding static tuning curve as a function of the IH current (green markers: experimental points; red dashed line: quadratic fit) and associated variation of the optical power (blue markers: Experimental points; blue dashed line: 3th order polynomial fit). The experimental data of the optical power were extracted from the measured transmission through the N_2O cell; the gaps in the data result from the presence of N_2O absorption lines that have been removed.
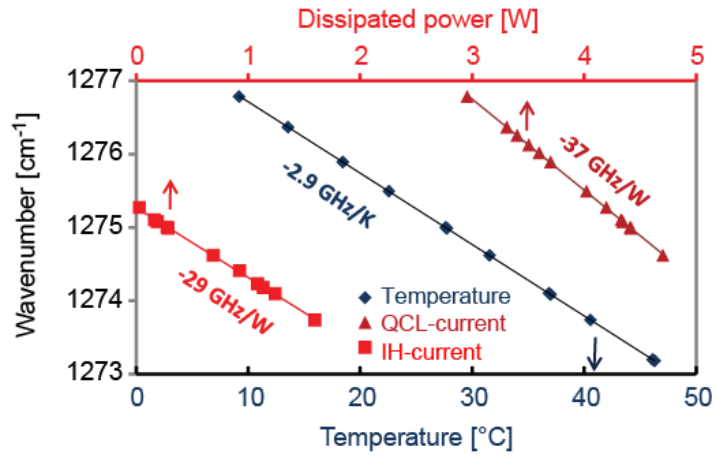
Figure 5.5: Static tuning coefficients of the QCL measured for temperature, QCL-current and IH-current tuning, respectively (markers: Experimental points; lines: Linear fits).

5.3.2 Tuning Speed

The tuning speed of the QCL has been determined from the frequency step response to a change of the injection current, IH current, and temperature, respectively. For this measurement, the laser was tuned to the side of a N_2O absorption line, as illustrated in Figure 5.6. The optical power transmitted through the gas absorption cell was monitored on an oscilloscope using a fast photodiode. A small step of current (1.2 mA for the QCL or 6.6 mA for the IH) or of temperature (0.16 K) was applied, producing a frequency change of approximately 500 MHz. The temporal evolution of the QCL frequency was linearly converted into a change of the transmitted optical power in the side of the absorption line.

The monitored signals were recorded on the oscilloscope and are displayed in Figure 5.7 (for a temperature step) and in Figure 5.8 (for a step of the QCL or IH current). Here, the frequency change resulting from
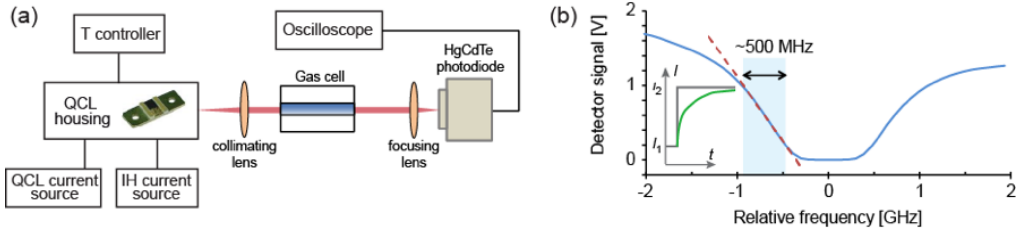
Figure 5.6: (a) Experimental principle of the QCL frequency step response measurement using an absorption line of N_2O; (b) the side of the absorption profile (blue curve) corresponding to the P11e line of N_2O at 1275.5 cm^{-1} acts as a frequency discriminator (dashed red line) that linearly converts the change of the laser frequency into a change of the transmitted optical power detected by a photodiode. A current step of the QCL, IH or TEC was applied (from I_1 to I_2, see inset) to produce an exponential frequency change (schematized by the green line) of approximately 500 MHz that was recorded by an oscilloscope.

a step of the IH current is nearly as fast as for a step of the injection current: a frequency step of 500 MHz is achieved in a similar timescale of a few milliseconds. In comparison, the temperature control with the TEC is approximately four orders of magnitude slower. The temporal response observed for a temperature step applied to the QCL sub-mount is well approximated by a single exponential decay with a long time constant of around 100 s (dashed line in Figure 5.7).

In contrast, the temporal response to a step of the QCL or IH current shows a very different behavior (Figure 5.8) characterized by a strong deviation from a single exponential response, which indicates that different thermal time constants are involved in the system. For a step of the QCL current, a very fast change of the optical frequency is first observed with a time constant $\tau_1 < 1$ µs, which is not completely resolved
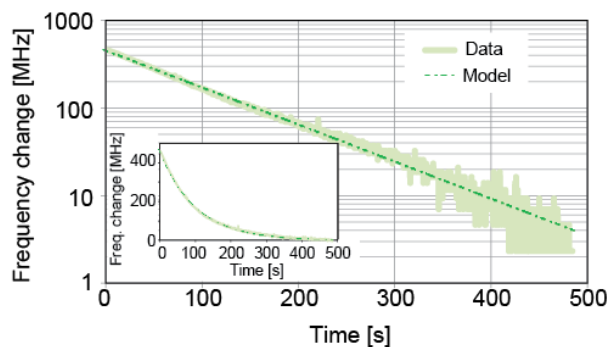
Figure 5.7: Temporal evolution of the QCL optical frequency measured for a step change of the TEC temperature of around 0.16 K, displayed in a semi-log scale. The inset shows a linear representation. The experimental data are well approximated by a single exponential decay with a time constant of around 100 s (dashed-dotted line).

in the plot. This very short time constant is attributed to the fast resulting heating of the QCL active zone. It is followed by another fairly fast change ($\tau_2 \approx 20$ µs), which is believed to result from the heat dissipation in the laser substrate. Then, it takes more time for the heat to dissipate into the copper sub-mount, and possibly in the soldering, as a result of their relatively high thermal inertia. This leads to two longer time constants $\tau_3 \approx 0.7$ ms and $\tau_4 \approx 4$ ms, respectively. These longer time constants are clearly visible in the semi-log plot of the QCL frequency evolution shown in Figure 5.8 (a).

For a change of the IH current, a similar temporal response is observed (Figure 5.8 (b)), which is dominated by the time constants $\tau_3 \approx 0.8$ ms and $\tau_4 \approx 4$ ms that are close to the case of the QCL current. However, the first two time constants are not as short ($\tau_1 \approx 8$ µs and $\tau_2 \approx 50$ µs, respectively). This results from the fact that the heat is not directly generated in the active region, but at some distance from it, and

66
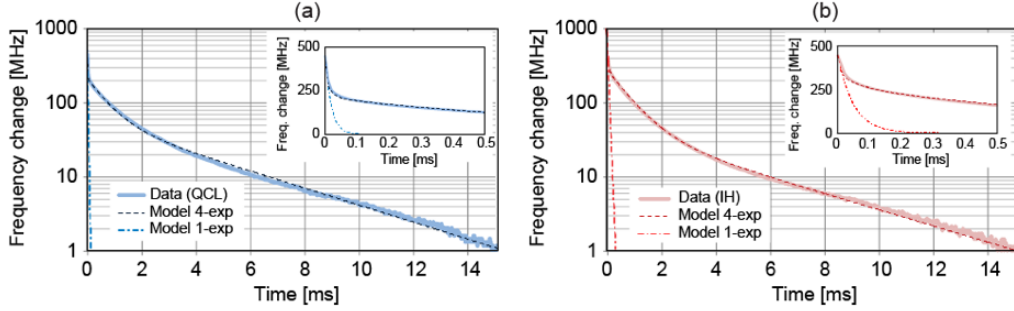
Figure 5.8: Temporal evolution of the QCL optical frequency measured for a step change of the QCL current (a) and IH current (b), displayed in a semi-log scale. The insets show a linear representation of the initial 0.5-ms decay. The temporal response does not correspond to a single exponential decay of time constant τ_2 (dashed-dotted lines), but is modelled by the sum of four decaying exponential terms (dashed lines).

some time is needed until the dissipated heat reaches the active region.

The cut-off frequency $f_i = 1/(2\pi\tau_i)$ associated to each of these time constants will be better identified in the measurement of the FM transfer functions of the laser presented in Subsection 5.3.3.

5.3.3 Frequency Modulation Response

The FM transfer functions obtained for a modulation of the QCL injection current or IH current are displayed in Figure 5.9 (in amplitude and phase) for different average IH currents. The FM response with respect to the QCL injection current modulation is independent of the IH current. For IH current modulation, the FM response (in terms of frequency tuning coefficient per unit of IH current, in GHz/mA) scales almost linearly with the average IH current as a result of the quadratic thermal response of the heater, previously shown in Figure 5.4 (b). If expressed per unit of

dissipated electrical power (in GHz/W), the tuning coefficient for the IH at low modulation frequency becomes nearly independent of the average IH current, on the order of 20 GHz/W that is in good agreement with the value previously obtained for the DC tuning coefficient. The FM response for QCL injection current shows a bandwidth of around 1 MHz, corresponding to a drop of 10 dB in amplitude and to an associated phase shift of 90°, a value that is acceptable in a feedback loop to stabilize the frequency of a QCL to an optical reference. For a modulation of the IH current, a bandwidth of around 100 kHz is typically achieved, defined in the same way as for the QCL current modulation.
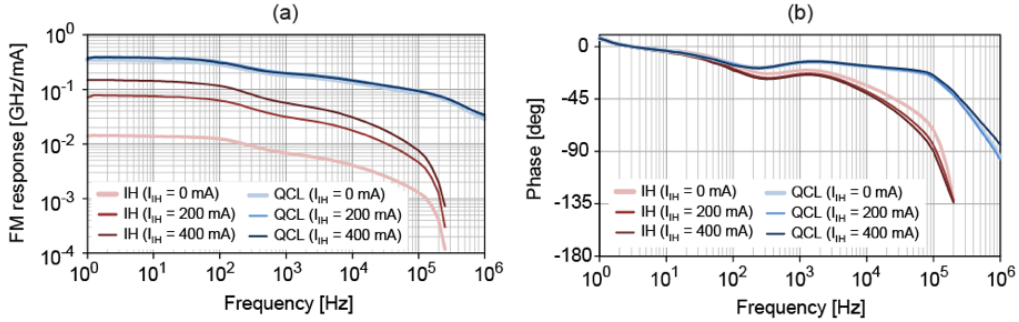
Figure 5.9: FM transfer function in amplitude (a) and phase (b) obtained for a modulation of the QCL-current (blue lines) and IH-current (red lines), both at different IH currents I_{IH}.

In order to investigate more quantitatively these FM transfer functions and get a deeper understanding of the observed dynamic responses, we modelled the thermal response $R(f)$ of the QCL (obtained by normalizing the dynamic FM response by its value at 1 Hz) by cascaded first-order low-pass filters that describe the heat extraction in different parts of the laser following the model previously used by Tombez et al. [80]. By considering that the output frequency of the laser is mainly determined by the

68

average temperature in the active region and that the applied current modulation (to the heater or active region) induces a proportional variation of the electrical power dissipated in the device, the measured FM responses, thus, also represent the laser thermal response $R(f)$:

$$R(f) = \frac{\Delta T}{\Delta P}(f) = \sum_i \frac{R_i}{1 + jf/f_i} \qquad (5.1)$$

In this equation, the R_i represent the thermal resistances and the f_i the characteristic frequencies (thermal cut-off frequencies) associated to the different parts of the laser, which also depend on the corresponding thermal capacities C_i:

$$f_i = \frac{1}{2\pi R_i C_i} \qquad (5.2)$$

This simple model was used to simultaneously fit the experimental data in magnitude and phase to determine the different time constants. In contrast to the model used in Reference [80], which made use of three different low-pass filters, we added here a 4th filter with a low cut-off frequency f_4 to take into account the longest time constant τ_4 previously observed in the step response shown in Figure 5.8. As this 4th filter was not clearly apparent in the measured transfer functions, its cut-off frequency $f_4 = 1/(2\pi\tau_4)$ was directly determined from the slow decay observed in the step response and was not considered as a free parameter in the fit. We also extracted the relative contribution r_i of the thermal resistance of each part of the QCL structure to the total thermal resistance:

$$r_i = \frac{R_i}{\sum_i R_i} \qquad (5.3)$$

The fitted model is plotted along with the measured frequency modulation responses in Figure 5.10 and shows a very good agreement in terms of amplitude and phase. The cut-off frequencies f_i retrieved from the fit for the modulation of the QCL and IH currents are listed in Table 5.1 together with the relative weight r_i of each filter. These frequencies were used in the modeled step responses displayed in Figure 5.8, which were also in good agreement with the experimental data. For the QCL current modulation, the highest cut-off frequency is around 220 kHz, whereas it is one order of magnitude lower for IH modulation. This results from the fact that the heat is generated at some distance from the active region with the IH, and the temperature of the active region cannot be changed as fast as with a change of the QCL current that acts directly onto the active region.
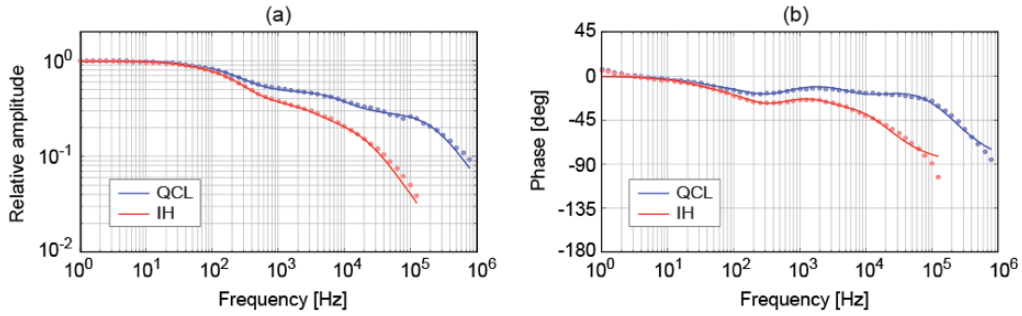
Figure 5.10: Relative FM response of the QCL obtained under direct modulation of the injection current (blue points) or IH current (red points) and fitted model (solid lines). Both amplitude (a) and phase (b) responses are shown. A global phase shift of 180° was added to all phase plots.

Modulation	f_1 (kHz)	r_1	f_2 (kHz)	r_2	f_3 (Hz)	r_3	f_4 (Hz)	r_4
QCL current	220	0.27	8.3	0.20	230	0.36	42	0.17
IH current	19.6	0.18	3.2	0.16	200	0.46	40	0.20

Table 5.1: Cut-off frequencies f_i and relative weights r_i of the different low-pass filters obtained from the fit of the transfer functions for QCL and IH current modulation. The frequency f_4 was fixed from the longest time constant τ_4 observed in the step response of Figure 5.8.

5.4 Preliminary Application in WMS

The IH offers an alternative channel to modulate the emission frequency of the QCL at a relatively high speed. A benefit of this actuator is the capability to act directly on the internal temperature of the active region, thus offering new possibilities to reduce the frequency noise of a QCL in an all-electrical configuration using the voltage noise measured between the QCL terminals as an error signal [86]. Another potential benefit of modulating the QCL frequency through the IH current is the reduced associated RAM that can be achieved in some conditions in comparison to the modulation of the QCL injection current. This property is attractive when using the first harmonic ($1f$) signal of a molecular or atomic absorption line obtained in WMS to frequency-stabilize a QCL. In this case, the RAM constitutes an undesired spurious effect that generally degrades the stabilization performance as a result of the background offset present in the $1f$ signal. The importance of this offset depends on several parameters, such as the ratio between the FM and AM indices of the laser, but also on the phase shift between AM and FM, and on the phase of the $1f$ demodulation.

The traditional injection current modulation used to modulate the frequency of a QCL is naturally accompanied by some RAM as the optical power scales linearly with the injection current. This RAM produces the background offset in the $1f$ signal of an absorption line, whose amplitude depends on the phase of the $1f$ demodulation. This phase can be adjusted to cancel out the offset component due to RAM [90], but this can lead at the same time to a strong reduction of the amplitude of the $1f$ signal of the absorption line (induced by the laser FM), depending on the phase shift between AM and FM. Modulating the IH current to generate a WMS signal is an alternative method that can present some advantages in terms of RAM. In contrast to the QCL injection current that directly influences the output power by changing the population inversion of the gain medium, the IH current has only an indirect effect on the output power via the induced temperature change. The resulting variation of the optical power is thus weaker and can reduce the RAM impact in WMS.

To illustrate the attractiveness of the IH current modulation for WMS, we present here a proof-of-principle experiment performed on a N_2O absorption line with a modulation of the IH current and we compare the results with the standard approach of injection current modulation. For this purpose, we modulated the QCL frequency with a 25-kHz sine wave signal applied either to the QCL injection current or to the IH current and we demodulated the photodiode signal detected at the output of the gas cell at the modulation frequency using a lock-in amplifier. In addition, the laser current was slowly swept with a triangular signal at 10 Hz to scan through the absorption line and the $1f$ signal was recorded on an oscilloscope during this sweep. Both the modulation depth and the phase of the lock-in detection were adjusted to maximize the amplitude of the $1f$

signal of the gas absorption line.
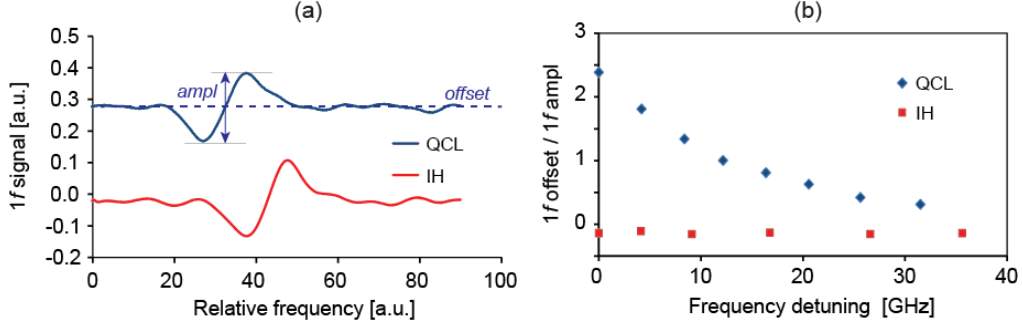
Figure 5.11: (a) Comparison of the first harmonic WMS signal of a N_2O line obtained for QCL injection current and IH current modulation (at T $\approx$ 20 °C and $I_{QCL} \approx$ 420 mA), showing the strongly reduced background offset obtained for IH current modulation; (b) ratio between the offset and the amplitude of the $1f$ signal obtained for QCL and IH modulation at different QCL (IH) currents, converted into a corresponding frequency detuning. For each value of the QCL (IH) current, the laser temperature was slightly varied to keep the laser frequency around the considered N_2O transition. At each DC current, the amplitude of the applied modulation was adjusted to maximize the peak-to-peak amplitude of the $1f$ signal.

The first harmonic WMS signals obtained for a modulation of the QCL injection current and of the IH current are shown in Figure 5.11 (a). Both curves were obtained for a QCL injection current of around 420 mA at a laser sub-mount temperature of around 20 °C. In the case of injection current modulation, no current was applied to the IH. For IH current modulation, a DC bias current of around 170 mA was applied on top of the modulation and the QCL temperature was slightly decreased by around 2 K to compensate for the resulting frequency shift of around 6 GHz and to keep the laser on the N_2O transition. The derivative signal of the absorp-

tion line sits on a background offset that directly results from the intensity modulation of the emitted light. This offset is large in the case of a modulation of the QCL injection current, as it directly modulates the laser gain and therefore the optical power. However, the relative importance of the RAM, and thus the magnitude of the background offset in the WMS $1f$ signal, has a significant dependence on the average QCL current: the relative magnitude of the offset decreases when the QCL injection current increases, as the relative power modulation is reduced accordingly, whereas the FM tuning coefficient has only a minor dependence. This relative reduction of the RAM is illustrated in Figure 5.11 (b), which shows the ratio between the background offset (arising from RAM) and the peak-to-peak amplitude of the spectroscopic component of the N_2O absorption line (arising from FM) in the detected $1f$ signal obtained for QCL and IH current modulation at different QCL (respectively IH) currents. For a modulation of the IH current, the offset in the $1f$ signal is tiny as the optical power varies only due to the resulting temperature change. The offset has also an opposite sign compared to the QCL current modulation, as the optical power decreases with increasing IH current as illustrated in Figure 5.4 (b), whereas it increases with the injection current. Furthermore, the relative magnitude of the background offset in the WMS $1f$ signal (and thus the importance of RAM) remains almost constant at any IH current, which illustrates the good decoupling between frequency and amplitude modulation when modulating the IH current.

5.5 Conclusion

In conclusion, we have characterized in detail a new frequency tuning actuator in a QCL emitting at 7.8 μm. A resistive IH placed in the vicinity of the active region can be electrically controlled, enabling fast changes of the internal temperature of the laser to be applied, which results in a fast control of the emission frequency. The laser output frequency has a linear dependence on the electrical power dissipated in the resistive heater and this frequency tuning occurs with a minor change of the emitted optical power. The impulse response of the laser frequency to a current step applied to the IH is as fast as for a step change of the QCL current and a frequency change of 500 MHz was achieved in a few milliseconds, limited by the head dissipation out of the active region towards the laser sub-mount. For a sine modulation, the QCL current remains approximatively one order of magnitude faster and enables frequency-modulating the QCL radiation with a bandwidth in the MHz range (corresponding to a drop in amplitude of around 10 dB and an associated phase shift of 90°), whereas the bandwidth is limited to around 100 kHz when modulating the IH current. A thermal model was presented to describe the transfer functions experimentally measured for a modulation of the QCL current and IH current. Four different time constants were determined and identified to the heat dissipation in different parts of the device. The shortest time constant is one order of magnitude shorter in the case of QCL current modulation, corresponding to a cut-off frequency higher than 200 kHz, compared to around 20 kHz for IH current modulation.

Nevertheless, the modulation bandwidth achieved with the IH is sufficient for most spectroscopic applications of QCLs, such as WMS for

trace gas sensing or laser stabilization. Modulating the IH current also has the further advantage of a reduced RAM compared to a direct modulation of the QCL current in some conditions. We showed a proof-of-principle demonstration of the benefit of this decoupled frequency/amplitude modulation in the case of the $1f$ signal of a N_2O absorption line, where the spectroscopic signal was almost free of background offset for a modulation of the IH current, whereas a higher offset was observed when modulating the QCL current. In this latter case, the relative magnitude of the background offset could be reduced by adjusting the phase of the demodulation, or by operating the QCL at a higher current. However, the first solution might also lead to a decrease of the amplitude of the absorption signal depending on the phase shift between AM and FM induced by the current modulation. For the modulation of the IH current, the relative background offset is fairly independent of the DC current, as both the optical frequency and output power of the QCL have a similar dependence on the IH current.

Finally, the new IH provides an additional channel to apply fast frequency corrections to a QCL for frequency stabilization and noise reduction. This is attractive to reduce the short-term linewidth of a QCL without using an optical reference such as a molecular transition, by directly exploiting the noise on the voltage between the QCL terminals, as previously demonstrated [86, 87]. Whereas a former implementation used an external near-infrared laser diode shining on the top surface of a QCL for fast control of the QCL internal temperature, the new IH provides a much more compact all-electrical solution that will be investigated in the future.

Chapter 6

Outlook and Future Scope

During the course of this doctoral study, my focus has been to develop and advance new generation laser sources for applications in metrology and spectroscopy. These applications are important in science and our lives. Metrology enables us to measure. It is essential in science. Frequency combs are the fast flourishing, new generation optical measurement tools. Spectroscopy enables the detection of atoms and molecules. It is a basic and important field, with the potential to improve our quality of life. Molecule detection by using a frequency comb or a QCL will enable us to map out pollution dispersion on our planet, to easily find out the sources of toxic gas leaks, to sense security or health risks in public areas, like airports. I aimed to bring the current technology to the next level; to enable easy to use and integrate, compact laser sources for metrology and spectroscopy.

Compact Ti:Sapphire lasers for microscopy

The most important property of the Ti:Sapphire laser is its wide spectral coverage. This enables tuning of the laser output to a desired wavelength of importance. In microscopy, such as for multi-photon imaging, the Ti:Sapphire laser has a crucial place. However, this has always been costly and complex. We achieved efficient and stable lasing from a green diode-pumped, mode-locked Ti:Sapphire laser, reaching 450 mW in average output power hitting an optical-to-optical efficinecy of 15%. This power level is sufficient for microscopy applications. An examplary picture of mouse intestine imaged by two photon excitation microscopy using a Ti:Sapphire laser is shown in Figure 6.1.
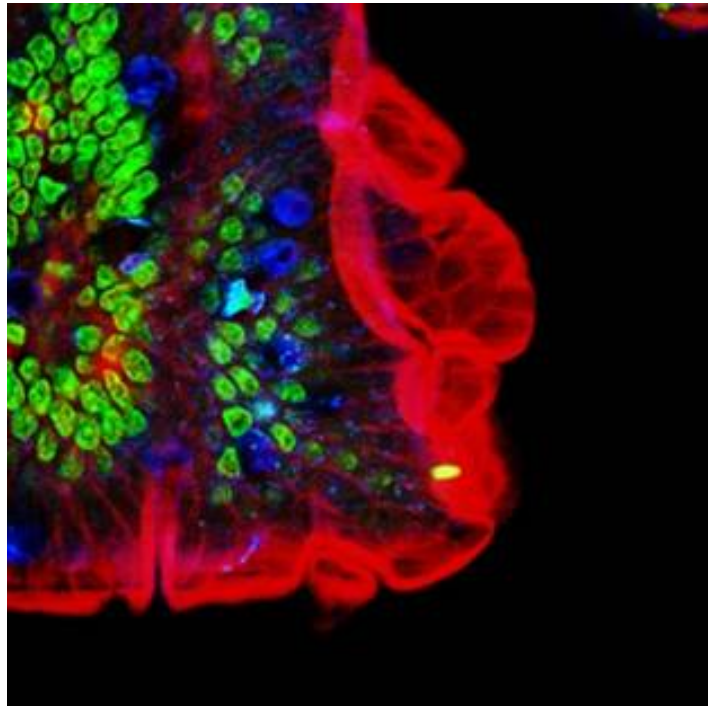

Figure 6.1: Cryostat section of mouse intestine imaged using a Ti:Sapphire laser through two photon excitation microscopy. [91]

In our lasers, we used two green laser diodes and pumped the laser crystal from both sides. Higher output powers can be further achieved by increasing the pump power through: spectral beam combining, using multiple pump diodes side by side, or fiber combining in multi-mode fibers. The low-cost of green laser diodes, currently as low as $130, is a significant advantage as compared to the other existing pumping solutions with an average cost of at least $5,000. The blue laser diodes entered the market with significantly high prices and now they cost around $10/W. It will be no surprise to see green laser diode prices falling down to the same level, owing to mass production. This will enable cheaper, simpler and compact Ti:Sapphire lasers available.

Compact frequency combs

Initial frequency combs were based on Ti:Sapphire lasers, until fiber lasers took over. Although the solid state lasers offer higher stability and lower noise than the fiber lasers, there were few disadvantageous that made the fiber systems a more suitable choice. The weak point of the Ti:Sapphire laser has been the pump lasers. They are complex costly and lacking in modulation capabilities, that is required for achieving high stability of the CEO. Although the Ti:Sapphire crystal has an upper state lifetime of 3.2 µm and allows modulation bandwidth of up to around 1 MHz [76], the complex pumping schemes have been the limiting factor, reducing the bandwidth to values around few kHz. Diode pumping can surpass this limitation. We stabilized the CEO frequency of our Ti:Sapphire laser by direct pump diode modulation, limited by the driver electronics. The quality of the stability can be further improved by using more suitable electronic cir-

cuits. Diode pumping greatly simplifies frequency comb generation from Ti:Sapphire lasers and we expect a strong come back.

The fiber based frequency combs are already at an advanced stage. However there is still need for fast and easy to implement CEO frequency actuators. Our development of OOM of a semiconductor chip in a fiber laser frequncy comb will attract attention as a better tool.

Metrology applications can greatly benefit from frequency combs with wider comb spacing, in the range of GHz levels. Solid state lasers can easily achieve this [92]. A next step to Ti:Sapphire frequency combs would be to make an ultra-compact GHz repetition rate Ti:Sapphire laser, pumped directly by tiny green laser diodes.

Compact, broadly tunable, stabilized QCLs

QCLs will play a very important role in the future of our environment. Their emission in the mid-IR region and fast technological advancement will enable them to be the perfect tool for environmental sensing. New types of QCLs based on Vernier effect are currently under development by Alpes Lasers [93]. These lasers extend the tuning range of the QCLs significantly, allowing broadband multi-species molecule detection. QCL and quantum cascade detector (QCD) hybrids have emerged [94] which can lead to chipscale standalone molecule sensors in the future.

Our work on the IH tunable QCL is an important addition to its capabilities. We achieved fast frequency tunability using this simple actuator, with minimal effects to the laser power. Another possible subject to investigate would be the reduction of the optical linewidth of the QCL

by using the IH as the actuator. This would further narrow down the linewidth with a minimalistic approach.

Bibliography

[1] T. H. Maiman, "Stimulated optical radiation in ruby," *Nature*, vol. 187, pp. 493–494, 1960.

[2] I. Newton, *Opticks*. 1704.

[3] C. Huygens, *Treatise on Light*. Pieter van der Aa, 1690.

[4] T. Young, "The bakerian lecture: On the theory of light and colours," *Philosophical Transactions of the Royal Society of London*, vol. 92, pp. 12–48, 1802.

[5] J. C. Maxwell, "A dynamical theory of the electromagnetic field," *Philosophical Transactions of the Royal Society of London*, vol. 155, pp. 459–512, 1865.

[6] M. Planck, "Zur theorie des gesetzes der energieverteilung im normalspectrum," *Verhandlungen der Deutschen Physikalischen Gesellschaft*, vol. 2, pp. 237–245, 1900.

[7] A. Einstein, "Zur elektrodynamik bewegter körper," *Annalen der Physik*, vol. 322, pp. 891–921, 1905.

[8] A. Einstein, "Strahlungs-emission und -absorption nach der quantentheorie," *Verhandlungen der Deutschen Physikalischen Gesellschaft*, vol. 18, pp. 318–323, 1916.

[9] N. Taylor, *LASER: The inventor, the Nobel laureate, and the thirty-year patent war.* Simon Schuster, 2000.

[10] P. P. Sorokin and M. J. Stevenson, "Stimulated infrared emission from trivalent uranium," *Phys. Rev. Lett.*, vol. 5, p. 557, 1960.

[11] A. Javan, W. R. Bennett, and D. R. Herriott, "Population inversion and continuous optical maser oscillation in a gas discharge containing a He-Ne mixture," *Phys. Rev. Lett.*, vol. 6, p. 106, 1961.

[12] J. E. Geusic, H. M. Marcos, and L. G. V. Uitert, "Laser oscillations in Nd-doped yttrium aluminum, yttrium gallium and gadolinium garnets," *Applied Physics Letters*, vol. 4, p. 182, 1964.

[13] C. K. N. Patel, "Continuous-wave laser action on vibrational-rotational transitions of CO_2," *Physical Review*, vol. 136, pp. A1187–A1193, 1964.

[14] R. N. Hall, G. E. Fenner, J. D. Kingsley, T. J. Soltys, and R. O. Carlson, "Coherent Light Emission From GaAs Junctions," *Physical Review Letters*, vol. 9, pp. 366–368, 1962.

[15] W. B. Bridges, "Laser oscillation in singly ionized Argon in the visible spectrum," *Appl. Phys. Lett.*, vol. 4, pp. 128–130, 1964.

[16] P. A. Crump, M. Grimshaw, J. Wang, W. Dong, S. Zhang, S. Das, J. Farmer, M. DeVito, L. S. Meng, and J. K. Brasseur, "85% Power Conversion Efficiency 975-nm Broad Area Diode Lasers at -50 °C, 76% at 10 °C," in *CLEO, paper JWB24*, 2006.

[17] J. Faist, F. Capasso, D. L. Sivco, C. Sirtori, A. L. Hutchinson, and A. Y. Cho, "Quantum cascade laser," *Science*, vol. 22, pp. 553–556, 1994.

[18] W. E. Lamb, "Theory of an optical laser," *Phys. Rev.*, vol. 134, p. A1429, 1964.

[19] M. E. Fermann, "Passive mode locking by using nonlinear polarization evolution in a polarization-maintaining erbium-doped fiber," *Opt. Lett.*, vol. 18, p. 894, 1993.

[20] U. Keller, K. J. Weingarten, F. X. Kaertner, D. Kopf, B. Braun, I. D. Jung, R. Fluck, C. Honninger, N. Matuschek, and J. A. der Au, "Semiconductor saturable absorber mirrors (SESAMs) for femtosecond to nanosecond pulse generation in solid-state lasers," *IEEE J. Sel. Top. Quantum Electron.*, vol. 2, p. 435, 1996.

[21] T. Brabec, "Kerr lens mode locking," *Opt. Lett.*, vol. 17, p. 1292, 1992.

[22] P. F. Moulton, "Spectroscopic and laser characteristics of Ti:Al$_2$O$_3$," *J. Opt. Soc. Am. B*, vol. 3, pp. 125–133, 1986.

[23] SPIE, "Youtube: Peter Moulton on the Ti:Sapphire laser." `https://www.youtube.com/watch?v=D4Ej0k6z_fc`.

[24] R. Ell, U. Morgner, F. X. Kärtner, J. G. Fujimoto, E. P. Ippen, V. Scheuer, G. Angelow, T. Tschudi, M. J. Lederer, A. Boiko, and B. Luther-Davies, "Generation of 5-fs pulses and octave-spanning spectra directly from a Ti:sapphire laser," *Optics Lett.*, vol. 26, pp. 373–375, 2001.

[25] U. Morgner, F. X. Kaertner, S. H. Cho, Y. Chen, H. A. Haus, J. G. Fujimoto, E. P. Ippen, V. Scheuer, G. Angelow, and T. Tschudi, "Sub-two-cycle pulses from a Kerr-lens mode-locked Ti:sapphire laser," *Optics Lett.*, vol. 24, pp. 411–413, 1999.

[26] L.-J. Chen, A. J. Benedick, J. R. Birge, M. Y. Sander, and F. X. Kaertner, "Octave-spanning, dual-output 2.166 GHz Ti:sapphire laser," *Optics Express*, vol. 16, pp. 20699–20705, 2008.

[27] S. A. Diddams, D. J. Jones, J. Ye, S. Cundiff, J. L. Hall, J. K. Ranka, R. S. Windeler, R. Holzwarth, T. Udem, and T. W. Hansch, "Direct Link

between Microwave and Optical Frequencies with a 300 THz Femtosecond Laser Comb," *Phys. Rev. Lett.*, vol. 84, pp. 5102–5105, 2000.

[28] A. S. K. F. Wall, "Titanium Sapphire lasers," *The Lincoln Laboratory Journal*, vol. 3, pp. 447–462, 1990.

[29] C. J. Koester and E. Snitzer, "Amplification in a fiber laser," *Applied Optics*, vol. 10, pp. 1182–1186, 1964.

[30] E. P. Ippen, C. V. Shank, and A. Dienes, "Passive mode locking of the cw dye laser," *Appl. Phys. Lett.*, vol. 21, pp. 348–350, 1972.

[31] M. E. Fermann, M. J. Andrejco, Y. Silberberg, and M. L. Stock, "Nonlinear amplifying loop mirror," *Opt. Lett.*, vol. 18, pp. 894–896, 1990.

[32] S. Y. Set, H. Yaguchi, Y. Tanaka, and M. Jablonski, "Laser mode locking using a saturable absorber incorporating carbon nanotubes," *J. Lightwave Technol.*, vol. 22, p. 51, 2004.

[33] J.-B. Lecourt, C. Duterte, F. Narbonneau, D. Kinet, Y. Hernandez, and D. Giannone, "All-normal dispersion, all-fibered pm laser mode-locked by sesam," *Opt. Express*, vol. 20, pp. 11918–11923, 2012.

[34] D. J. Richardson, J. Nilsson, and W. A. Clarkson, "High power fiber lasers: current status and future perspectives [invited]," *J. Opt. Soc. Am. B*, vol. 27, pp. B63–B92, 2010.

[35] T. W. Hänsch, "Nobel Lecture: Passion for precision," *Rev. Mod. Phys.*, vol. 78, pp. 1297–1309, Nov 2006.

[36] J. L. Hall, "Nobel Lecture: Defining and measuring optical frequencies," *Rev. Mod. Phys.*, vol. 78, pp. 1279–1295, Nov 2006.

[37] S. Schilt and T. Südmeyer, "Carrier-Envelope Offset Stabilized Ultrafast Diode-Pumped Solid-State Lasers," *Appl. Sci.*, vol. 5, pp. 787–816, 2015.

[38] D. J. Jones, S. A. Diddams, J. K. Ranka, A. Stentz, R. S. Windeler, J. L. Hall, and S. T. Cundiff, "Carrier-envelope phase control of femtosecond mode-locked lasers and direct optical frequency synthesis," *Science*, vol. 288, pp. 635–639, 2000.

[39] H. R. Telle, G. Steinmeyer, A. E. Dunlop, J. Stenger, D. H. Sutter, and U. Keller, "Carrier-envelope offset phase control: A novel concept for absolute optical frequency measurement and ultrashort pulse generation," *Appl. Physics B*, vol. 69, pp. 327–332, 1999.

[40] A. Apolonski, A. Poppe, G. Tempea, C. Spielmann, T. Udem, R. Holzwarth, T. W. Hänsch, and F. Krausz, "Controlling the phase evolution of few-cycle light pulses," *Phys. Rev. Lett.*, vol. 85, pp. 740–743, Jul 2000.

[41] T. Udem, R. Holzwarth, and T. W. Hansch, "Optical frequency metrology," *Nature*, vol. 416, pp. 233–237, 2002.

[42] C. Benko, A. Ruehl, M. J. Martin, K. S. E. Eikema, M. E. Fermann, I. Hartl, and J. Ye, "Full phase stabilization of a Yb:fiber femtosecond frequency comb via high-bandwidth transducers," *Opt. Lett.*, vol. 37, pp. 2196–2198, Jun 2012.

[43] C.-C. Lee, C. Mohr, J. Bethge, S. Suzuki, M. E. Fermann, I. Hartl, and T. R. Schibli, "Frequency comb stabilization with bandwidth beyond the limit of gain lifetime by an intracavity graphene electro-optic modulator," *Opt. Lett.*, vol. 37, pp. 3084–3086, 2012.

[44] M. Hoffmann, S. Schilt, and T. Südmeyer, "CEO stabilization of a femtosecond laser using a SESAM as fast opto-optical modulator," *Opt. Express*, vol. 21, pp. 30054–30064, 2013.

[45] S. Hakobyan, V. J. Wittwer, K. Gurel, A. S. Mayer, S. Schilt, U. Keller, and T. Sudmeyer, "Carrier-envelope offset stabilization of a GHz repetition rate

femtosecond laser using opto-optical modulation of a SESAM," *submitted to Opt. Lett.*, 2017.

[46] B. P. Stoicheff, "Present status of the laser revolution in spectroscopy," in *Laser Spectroscopy III. Springer Series in Optical Sciences*, 1977.

[47] A. Schliesser, N. Picqué, and T. W. Hänsch, "Mid-infrared frequency combs," *Nature Photonics*, vol. 6, pp. 440–449, 2012.

[48] U. Keller, "Ultrafast solid-state laser oscillators: a success story for the last 20 years with no end in sight," *Appl. Phys. B*, vol. 100, pp. 15–28, 2010.

[49] W. Drexler, U. Morgner, R. K. Ghanta, F. X. Kaertner, J. S. Schuman, and J. G. Fujimoto, "Ultrahigh-resolution ophthalmic optical coherence tomography," *Nat. Med.*, vol. 7, pp. 502–507, 2001.

[50] V. M. Baev, T. Latz, and P. E. Toschek, "Laser intracavity absorption spectroscopy," *Appl. Phys. B*, vol. 69, pp. 171–202, 1999.

[51] C. Xu and W. W. Webb, "Measurement of two-photon excitation cross sections of molecular fluorophores with data from 690 to 1050 nm," *J. Opt. Soc. Am. B*, vol. 13, pp. 481–491, 1996.

[52] C. Xu, W. Zipfel, J. B. Shear, R. M. Williams, and W. W. Webb, "Multiphoton fluorescence excitation: New spectral windows for biological nonlinear microscopy," *Proc. Natl. Acad. Sci. USA*, vol. 93, pp. 10763–10768, 1996.

[53] H. Kneipp, J. Kolenda, P. Rairoux, B. Stein, D. Weidauer, J.-P. Wolf, and L. H. Woeste, "Ti:sapphire-laser-based lidar systems," *SPIE Proc.*, vol. 1714, p. 270, 1992.

[54] U. Keller, "Femtosecond to attosecond optics," *IEEE Photonics J.*, vol. 2, pp. 225–228, 2010.

[55] M. Drescher, M. Hentschel, R. Kienberger, G. Tempea, C. Spelmann, G. A. Reider, P. B. Corkum, and F. Krausz, "X-ray pulses approaching attosecond frontier," *Science*, vol. 291, pp. 1923–1927, 2001.

[56] B. Resan, E. Coadou, S. Petersen, A. Thomas, P. Walther, R. Viselga, J.-M. Heritier, J. Chilla, W. Tulloch, and A. Fry, "Ultrashort pulse Ti:sapphire oscillators pumped by optically pumped semiconductor (OPS) pump lasers," *SPIE Proc.*, vol. 6871, p. 687116, 2008.

[57] A. Vernaleken, B. Schmidt, M. Wolferstetter, T. W. Hänsch, R. Holzwarth, and P. Hommelhoff, "Carrier-envelope frequency stabilization of a Ti:sapphire oscillator using different pump lasers," *Opt. Express*, vol. 20, pp. 18387–18396, 2012.

[58] N. R. Newbury and W. C. Swann, "Low-noise fiber-laser frequency combs (Invited)," *J. Opt. Soc. Am. B*, vol. 24, pp. 1756–1770, 2007.

[59] N. Shuji, S. Masayuki, S. Nagahama, I. Naruhito, Y. Takao, M. Toshio, K. Hiroyuki, and S. Yasunobu, "InGaN-based multi-quantum-well-structure laser diodes," *Jpn. J. Appl. Phys.*, vol. 35, p. L74, 1996.

[60] P. W. Roth, A. J. Maclean, D. Burns, and A. J. Kemp, "Directly diode-laser-pumped Ti:sapphire laser," *Opt. Lett.*, vol. 34, pp. 3334–3336, 2009.

[61] P. W. Roth, A. J. Maclean, D. Burns, and A. J. Kemp, "Direct diode-laser pumping of a mode-locked Ti:sapphire laser," *Opt. Lett.*, vol. 36, pp. 304–306, 2011.

[62] P. W. Roth, D. Burns, and A. J. Kemp, "Power scaling of a directly diode-laser-pumped Ti:sapphire laser," *Opt. Express*, vol. 20, pp. 20630–20634, 2012.

[63] C. G. Durfee, T. Storz, J. Garlick, S. Hill, J. A. Squier, M. Kirchner, G. Taft, K. Shea, H. Kapteyn, M. Murnane, and S. Backus, "Direct diode-pumped

Kerr-lens mode-locked Ti:sapphire laser," *Opt. Express*, vol. 20, pp. 13677–13683, 2012.

[64] M. D. Young, S. Backus, C. Durfee, and J. Squier, "Multiphoton imaging with a direct-diode pumped femtosecond Ti:sapphire laser," *J. Microsc.*, vol. 249, pp. 83–86, 2013.

[65] H. Tanaka, R. Sawada, R. Kariyama, A. Hosaka, K. Hirosawa, and F. Kannari, "Power Scaling of Modelocked Ti:sapphire Laser Pumped by High Power InGaN Green Laser Diode," in *CLEO Europe, paper CA62*, 2015.

[66] S. Sawai, A. Hosaka, H. Kawauchi, K. Hirosawa, and F. Kannari, "Demonstration of a Ti:sapphire mode-locked laser pumped directly with a green diode laser," *Appl. Phys. Express*, vol. 7, pp. 022702–1–3, 2014.

[67] A. Rohrbacher, O. E. Olarte, V. Villamaina, P. Loza-Alvarez, and B. Resan, "Multiphoton imaging with blue-diode-pumped SESAM-modelocked Ti:Sapphire oscillator generating 5 nj 82 fs pulses," *Opt. Express*, vol. 25, pp. 10677–10684, May 2017.

[68] S. Backus, M. Kirchner, C. Durfee, M. Murnane, and H. Kapteyn, "Direct diode-pumped Kerr Lens 13 fs Ti:sapphire ultrafast oscillator using a single blue laser diode," *Opt. Express*, vol. 25, pp. 12469–12477, May 2017.

[69] S. Masui, T. Miyoshi, T. Yanamoto, and S. Nagahama, "1 W AlInGaN Based Green Laser Diodes," in *CLEO Pacific Rim, paper WH3-1*, 2013.

[70] M. C. Stowe, M. J. Thorpe, A. Pe'er, J. Ye, J. E. Stalnaker, V. Gerginov, and S. A. Diddams, "Direct frequency comb spectroscopy," *Advances in Atomic, Molecular, and Optical Physics*, vol. 55, pp. 1–60, 2008.

[71] C.-H. Li, A. J. Benedick, P. Fendel, A. G. Glenday, F. X. Kärtner, D. F. Phillips, D. Sasselov, A. Szentgyorgyi, and R. L. Walsworth, "A laser fre-

quency comb that enables radial velocity measurements with a precision of 1 cm s^{-1}," *Nature*, vol. 452, pp. 610–612, 2008.

[72] T. Steinmetz, T. Wilken, C. Araujo-Hauck, R. Holzwarth, T. W. Hansch, L. Pasquini, A. Manescau, S. D'Odorico, M. T. Murphy, T. Kentischer, W. Schmidt, and T. Udem, "Laser frequency combs for astronomical observations," *Science*, vol. 321, pp. 1335–1337, 2008.

[73] T. M. Fortier, M. S. Kirchner, F. Quinlan, J. Taylor, J. C. Bergquist, T. Rosenband, N. Lemke, A. Ludlow, Y. Jiang, C. W. Oates, and S. A. Diddams, "Generation of ultrastable microwaves via optical frequency division," *Nat. Photonics*, vol. 5, pp. 425–429, 2011.

[74] S. A. Diddams, T. Udem, J. C. Bergquist, E. A. Curtis, R. E. Drullinger, L. Hollberg, W. M. Itano, W. D. Lee, C. W. Oates, K. R. Vogel, and D. J. Wineland, "An optical clock based on a single trapped ^{199}Hg$^+$ ion," *Science*, vol. 293, pp. 825–828, 2001.

[75] D. T. Reid, C. M. Heyl, R. R. Thomson, R. Trebino, G. Steinmeyer, H. H. Fielding, R. Holzwarth, Z. Zhang, P. Del'Haye, T. Südmeyer, G. Mourou, T. Tajima, D. Faccio, F. Harren, and G. Cerullo, "Roadmap on ultrafast optics," *Journal of Optics*, vol. 18, p. 093006, 2016.

[76] R. P. Scott, T. D. Mulder, K. A. Baker, and B. H. Kolner, "Amplitude and phase noise sensitivity of modelocked Ti:sapphire lasers in terms of a complex noise transfer function," *Opt. Express*, vol. 15, pp. 9090–9095, 2007.

[77] G. D. Domenico, S. Schilt, and P. Thomann, "Simple approach to the relation between laser frequency noise and laser line shape," *Appl. Opt.*, vol. 49, pp. 4801–4807, 2010.

[78] J. Faist, C. Gmachl, F. Capasso, C. Sirtori, D. Sivco, J. Baillargeon, and A. Cho, "Distributed feedback quantum cascade lasers," *Appl. Phys. Lett.*, vol. 70, pp. 2670–2672, 1997.

[79] R. Maulini, M. Beck, J. Faist, and E. Gini, "Broadband tuning of external cavity bound-to-continuum quantum-cascade lasers," *Appl. Phys. Lett.*, vol. 84, pp. 1659–1661, 2004.

[80] L. Tombez, F. Cappelli, S. Schilt, G. Domenico, S. Bartalini, and D. Hofstetter, "Wavelength tuning and thermal dynamics of continuous-wave mid-infrared distributed feedback quantum cascade lasers," *Appl. Phys. Lett.*, vol. 103, p. 31111, 2013.

[81] J. Supplee, E. Whittaker, and W. Lenth, "Theoretical description of frequency modulation and wavelength modulation spectroscopy," *Appl. Opt.*, vol. 33, pp. 6294–6302, 1994.

[82] G. Bjorklund, "Frequency-modulation spectroscopy: A new method for measuring weak absorptions and dispersions," *Opt. Lett.*, vol. 5, pp. 15–17, 1980.

[83] M. Sigrist, "Trace gas monitoring by laser photoacoustic spectroscopy and related techniques (plenary)," *Rev. Sci. Instrum.*, vol. 74, pp. 486–490, 2003.

[84] A. Bismuto, Y. Bidaux, C. Tardy, R. Terazzi, T. Gresch, J. Wolf, S. Blaser, A. Muller, and J. Faist, "Extended tuning of mid-IR quantum cascade lasers using integrated resistive heaters," *Opt. Express*, vol. 23, pp. 29715–29722, 2015.

[85] S. Schilt, L. Tombez, C. Tardy, A. Bismuto, S. Blaser, R. Maulini, R. Terazzi, M. Rochat, and Südmeyer, "An experimental study of noise in mid-infrared quantum cascade lasers of different designs," *Appl. Phys. B*, vol. 119, pp. 189–201, 2015.

[86] L. Tombez, S. Schilt, D. Hofstetter, and S. T., "Active linewidth-narrowing of a mid-infrared quantum cascade laser without optical reference," *Opt. Lett.*, vol. 38, pp. 5079–5082, 2013.

[87] I. Sergachev, R. Maulini, A. Bismuto, S. Blaser, T. Gresch, Y. Bidaux, A. Müller, S. Schilt, and T. Südmeyer, "All-electrical frequency noise reduction and linewidth narrowing in quantum cascade lasers," *Opt. Lett.*, vol. 39, pp. 6411–6414, 2014.

[88] L. Tombez, S. Schilt, J. Francesco, T. Führer, B. Rein, T. Walther, G. Domenico, D. Hofstetter, and P. Thomann, "Linewidth of a quantum-cascade laser assessed from its frequency noise spectrum and impact of the current driver," *Appl. Phys. B*, vol. 109, pp. 407–414, 2012.

[89] L. Rothman, I. Gordon, Y. Babikov, A. Barbe, D. Benner, P. Bernath, M. Birk, L. Bizzocchi, V. Boudon, L. Brown, *et al.*, "The HITRAN2012 molecular spectroscopic database," *J. Quant. Spectrosc. Radiat. Transf.*, vol. 130, pp. 4–50, 2013.

[90] S. Schilt, L. Thévenaz, and P. Robert, "Wavelength modulation spectroscopy: Combined frequency and intensity laser modulation," *Appl. Opt.*, vol. 42, pp. 6728–6738, 2003.

[91] A. Diaspro, P. Bianchini, G. Vicidomini, M. Faretta, P. Ramoino, and C. Usai, "Multi-photon excitation microscopy," *Medical Engineering On-Line*, vol. 5, 2006.

[92] S. Hakobyan, V. J. Wittwer, P. Brochard, K. Gurel, S. Schilt, A. S. Mayer, U. Keller, and T. Sudmeyer, "Full stabilization and characterization of an optical frequency comb from a diode-pumped solid-state laser with GHz repetition rate," *Opt. Express*, vol. 25, pp. 20437–20453, 2017.

[93] Y. Bidaux, A. Bismuto, C. Tardy, R. Terazzi, T. Gresch, S. Blaser, A. Muller, and J. Faist, "Extended and quasi-continuous tuning of quan-

tum cascade lasers using superstructure gratings and integrated heaters,"
Applied Physics Letters, vol. 107, p. 221108, 2015.

[94] B. Schwarz, P. Reininger, D. Ristanić, H. Detz, A. M. Andrews, W. Schrenk, and G. Strasser, "Monolithically integrated mid-infrared lab-on-a-chip using plasmonics and quantum cascade structures," *Nature Communications*, vol. 5:4085, 2014.

Acronyms

AOM Acousto-optic modulator
AR Active region
BP Brewster plate
BPF Band pass filter
CEO Carrier envelope offset
CW Continuous wave
DBR Distributed Bragg reflector
DCM Dichroic mirror
DFB Distributed feedback
DM Dispersive mirror
DPSSL Diode pumped solid state laser
EOM Electro-optic modulator
FM Frequency modulation
FN Frequency noise
FOM Figure of merit
FWHM Full width half maximum
GTI Gires-Tournois interferometer
HR Highly reflective
HWP Half-wave plate
IH Integrated heater
IR Infrared
KLM Kerr lens modelocking
LLH Laser laboratory housing
LTF Laboratoire Temps-Fréquence
NPR Nonlinear polarization rotation
NTC Negative temperature coefficient
OC Output coupler
OOM Opto-optical modulation
PAS Photoacoustic spectroscopy
PBS Polarizing beam splitter
PCF Photonic crystal fiber

PID Proportional-Integral-Derivative
PM Polarization maintaining
PN Phase noise
PPLN Periodically poled lithium niobate
QCD Quantum cascade detector
QCL Quantum cascade laser
QWP Quarter-wave plate
RAM Residual amplitude modulation
RBW Resolution bandwidth
RF Radio frequency
RIN Relative intensity noise
RMS Root mean square
ROC Radius of curvature
SA Saturable absorber
SEM Scanning electron microscope
SESAM Semiconductor saturable absorber mirror
SHG Second harmonic generation
SNR Signal to noise ratio
SSB Single side band
TEC Temperature controller
VECSEL Vertical external cavity semiconductor laser
WDM Wavelength-division multiplexer
WMS Wavelength modulation spectroscopy

Curriculum Vitae

Name	Kutan Gürel
Date of Birth	28/09/1986
Nationality	Turkey

Education

2013-present	Doctoral studies at University of Neuchâtel, Switzerland
2011-2013	Master studies at Bilkent University, Ankara, Turkey
2007-2011	Bachelor studies at Bilkent University, Ankara, Turkey

Research Experience

2013-present	Research assistant at Laboratoire Temps-Fréquence, University of Neuchâtel, Neuchâtel, Switzerland
2008-2013	Research assistant at Ultrafast Optics Laboratory, Bilkent University, Ankara, Turkey
2011	Guest researcher at Laser Zentrum Hannover, Germany
2010	Guest researcher at Elettra Sincrotrone Trieste, Italy
2009	Guest researcher at DESY, Hamburg, Germany

Acknowledgement

I thank,

Thomas, for his support of my self development and (sometimes crazy) ideas, for his trust in my abilities and capability, for helping me build my first solid state laser at late night, and for his kind generosity.

Stéphane, for always finding time to share his deep knowledge and supporting me with the QCL work.

Sargis, for being a good friend and initiating numerous scientific discussions.

Nayara, for generously sharing her stuff in the lab and willingness to help for urgent deadlines.

Valentin, for his informative approach and high-end technical support.

Clément, for always being ready to party.

Loïc, for being a joyful office mate.

Bertrand, Maxim, Norbert, François, Pierre, William, Nil, Renaud and other LTF members, for being fun colleages.

Martin and Clara, for having fruitful and open scientific discussions.

Lionel, for teaching me about QCLs and being fun to work with.

Natacha, Joelle and Sandrine, for always being helpful.

Lumentum Switzerland and Alpes Lasers, for generosly lending me useful optical components and lasers.

My parents, Muazez and Hilmi, and my sister Merve, for their continuous support.

My wife Olga, for her never ending support and love and for being patient and understanding of my late night lab camps.